Atmospheric aerosols in Rome, Italy: Sources, dynamics and spatial variations during two seasons

Caroline Struckmeier[1], Frank Drewnick[1], Friederike Fachinger[1], Gian Paolo Gobbi[2] and Stephan Borrmann[1, 3]

[1]{Particle Chemistry Department, Max Planck Institute for Chemistry, Mainz, Germany}

[2]{Institute of Atmospheric Sciences and Climate, ISAC-CNR, Roma, Italy}

[3]{Institute for Atmospheric Physics, Johannes Gutenberg University, Mainz, Germany}

Correspondence to: C. Struckmeier (c.struckmeier@mpic.de), F. Drewnick (frank.drewnick@mpic.de)

Abstract

Investigations on atmospheric aerosols and their sources were performed during October/November 2013 and May/June 2014 subsequently in a suburban area of Rome (Tor Vergata) and in central Rome (near St. Peter's Basilica). During both years a Saharan dust advection event temporarily increased PM_{10} concentrations at ground level by approximately 10 µg m^{-3}. Generally, during Oct/Nov the ambient aerosol was more strongly influenced by primary emissions, whereas higher relative contributions of secondary particles (sulphate, aged organic aerosol) were found during May/June. Absolute concentrations of anthropogenic emission tracers (e.g. NO_x, CO_2, particulate polyaromatic hydrocarbons, traffic-related organic aerosol) were generally higher at the urban location. Positive matrix factorisation was applied to the PM_1 organic aerosol (OA) fraction of aerosol mass spectrometer (HR-ToF-AMS) data in order to identify different sources of primary OA (POA): traffic, cooking, biomass burning, and (local) cigarette smoking. While biomass burning OA was only found at the suburban site, where it accounted for the major fraction of POA (18-24 % of total OA), traffic and cooking were more dominant sources at the urban site. A particle type associated with cigarette smoke emissions, which is associated with a potential characteristic marker peak (*m/z* 84, $C_5H_{10}N^+$, a nicotine fragment) in the mass spectrum, was only found in central Rome, where it was emitted in close vicinity to the measurement location. Regarding secondary OA, in Oct/Nov, only a very aged, regionally advected oxygenated OA was found,

Atmospheric
Chemistry
and Physics
Discussions

1   which contributed 42-53 % to the total OA. In May/June total oxygenated OA accounted for

2   56–76 % of the OA. Here also a fraction (18-26 % of total OA) of a fresher, less oxygenated

3   OA of more local origin was observed. New particle formation events were identified from

4   measured particle number concentrations and size distributions during May/June 2014 at both

5   sites. While they were observed every day at the urban location, at the suburban location they

6   were only found under favourable meteorological conditions, but independent of advection of

7   the Rome emission plume. Particles from sources in the metropolitan area of Rome and

8   particles advected from outside Rome contributed 42-70 % and 30-58 % to total measured

9   PM_1, respectively. Apart from the general aerosol characteristics, in this study the properties

10   (e.g. emission strength) and dynamics (e.g. temporal behaviour) of each identified aerosol

11   type is investigated in detail in order to provide a better understanding of the observed

12   seasonal and spatial differences.

13

1   Introduction

15   Atmospheric aerosol particles remain a major uncertainty in both, estimations of climate

16   change (Boucher et al., 2013) and of impact of air pollution on public health (Heal et al.,

17   2012), and therefore are a major topic of current research (Fuzzi et al., 2015). Identifying the

18   sources, properties and concentrations of atmospheric particles is essential for evaluating their

19   effect on climate and health and constitutes a crucial step in finding measures for the

20   improvement of air quality.

21   Many studies on aerosols and their sources have been performed in urban environments (e.g.

22   Freutel et al., 2013; Mohr et al., 2012; Zheng et al., 2005), which are characterized by high

23   population densities and a large diversity of particle sources. Typical urban aerosol sources

24   include road traffic, cooking, and heating activities. Also emissions from biomass burning can

25   be important, both of regional origin (e.g., agricultural and wild fires; Reche et al., 2012), and

26   from residential wood combustion, which recently has become more prominent in Europe

27   even in urban environments (Fuller et al., 2013).

28   Many of these anthropogenic sources emit large amounts of organic material in the fine

29   particle fraction (e.g. Hildemann et al., 1991). In recent studies of particle source

30   identification (e.g. Allan et al., 2010; Mohr et al., 2012; Reche et al., 2012), positive matrix

31   factorisation (PMF) was applied to separate the organic aerosol (OA) fraction into different

32   factors associated with various OA sources, thereby providing indications about the fraction

Atmospheric
Chemistry
and Physics
Discussions

1   of primary and secondary organic aerosol (POA and SOA) (Zhang et al., 2011). Oxygenated

2   organic aerosol (OOA), mainly associated with SOA, is typically found to be the most

3   abundant fraction of OA (Lanz et al., 2010), with concentrations depending on season and

4   location (Zhang et al., 2011). Several studies, mainly such from observations during summer

5   time (Lanz et al., 2010), show discrimination of OOA into a fresher and a more aged type of

6   OOA based on different states of oxygenation and/or volatility (Jimenez et al., 2009).

7   While AMS measurements yield useful information on the age of OA, they cannot provide

8   evidence for new particle formation of fresh secondary aerosol. Indications for such, however,

9   can be found in physical aerosol properties like particle number concentration or size

10   distributions (e.g. Alam et al., 2003). New particle formation events in urban environments

11   have been investigated previously in several studies (e.g. Alam et al., 2003; Brines et al.,

12   2015; Minguillon et al., 2015; Shi et al., 2001; Zhang et al., 2004), and especially in the early

13   afternoon seem to be responsible for elevated particle number concentrations in urban areas in

14   Southern Europe (Reche et al., 2011).

15   On the other hand, while the health impact of coarse particles (PM_{10}-$PM_{2.5}$) is not yet fully

16   understood (Heal et al., 2012), the association between Saharan dust advections and

17   mortality/hospitalisation is quite well demonstrated (Stafoggia et al., 2016). Deserts are large

18   sources for mineral dust, which can strongly contribute to atmospheric PM_{10} levels, especially

19   in Southern Europe. Measurements performed in the period 2001-2004 during Saharan dust

20   advections over Rome showed a mean Saharan dust contribution of 12-16 $\mu g\ m^{-3}$ to daily

21   PM_{10} concentrations, leading to an average annual increase of about 2 $\mu g\ m^{-3}$ (Gobbi et al.,

22   2013). In the central Mediterranean region, maximum dust concentrations are typically

23   observed from spring to autumn (Barnaba and Gobbi, 2004).

24   In this study, we investigate the occurrence and properties of ambient aerosol from different

25   types of sources in Rome, which apart from local emissions can be influenced by advected

26   aerosol from continental Europe and the Sahara desert. During two different seasons (Oct/Nov

27   2013 and May/June 2014) and at two different locations (city centre and suburb), stationary

28   measurements of chemical and physical properties of aerosols, several trace gases, and

29   meteorological variables were performed. Non-refractory components of submicron particles

30   were measured with an Aerodyne high-resolution time-of-flight aerosol mass spectrometer

31   (HR-ToF-AMS). To support identification of particle sources, their strength and temporal

32   behaviour, the OA measured with the HR-ToF-AMS was further separated into different

33   factors using PMF.

1 Based on these measurements, in this work the urban atmosphere of Rome is investigated in

2 terms of particle source identification with a special focus on seasonal and spatial differences

3 influencing the presence and/or the characteristics of aerosol types in the city area.

4

5 **2 Experimental**

6 **2.1 Measurement locations and periods**

7 Measurement results presented in this study were obtained during four intensive field

8 campaigns in the greater Rome area, Italy (Table 1). The city of Rome covers an area of

9 1300 km^2 and has a population of about 2.9 million residents (about 4.3 million residents

10 within the whole metropolitan area of 5350 km^2). Three airports are located in the Rome

11 province, including the largest one in Italy (Fiumicino). Heavy industries are not found in

12 Rome; the economy is mainly based on services, education, construction, tourism, etc. Parks

13 and gardens cover some 34 % of the city area. Rome is characterised by high traffic volume

14 and density: about 50 % of the population commutes every day, mainly by private cars. The

15 cars per capita ratio in the city is 550 per 1000 inhabitants.

16 Measurements referred to as DIAPASON were performed during Oct/Nov 2013 and

17 May/June 2014 at the Institute of Atmospheric Sciences and Climate (CNR-ISAC) in Tor

18 Vergata, Rome. The institute is located in the south-eastern outskirts of Rome

19 (41°50'30.2''N, 12°38'51.2''E, 103 m a.s.l., 14 km from central Rome) and considered an

20 urban background site. The measurement platform MoLa (see Sect. 2.2) was positioned at a

21 free field with no buildings within a radius of 200 m. A frequently used street is located at

22 approximately 100 m distance in northern direction. The closest highway (A1) is situated

23 south-westerly at a distance of about 700 m. Single-house villages are scattered over this

24 territory, starting some 1 km from the site. Frascati, a town on the Alban Hills, is located at

25 about 4 km distance in south-easterly direction. During both periods measurements at Tor

26 Vergata were supported by the EC-LIFE+ project DIAPASON (Desert-dust Impact on Air

27 quality through model-Predictions and Advanced Sensors ObservatioNs), which aims on

28 improving existing tools to assess the contribution of Saharan dust to local PM$_{10}$ levels

29 (http://www.diapason-life.eu/, last access 09.05.2016). For this reason measurements were

30 scheduled in periods where a dust advection event could be expected and was forecasted by a

31 number of dust forecasts such as the DREAM8b (Basart et al., 2012), the SKIRON (Kallos et

32 al., 1997) and the Tel Aviv University (Alpert et al., 2002) models.

1 The "POPE" (Particle Observations around St. PEter's) measurement campaigns were

2 conducted during November 2013 and June 2014 in central Rome. Measurements were

3 performed inside a courtyard belonging to the administration of the hospital "Santo Spirito"

4 (41°54'04.3"N, 12°27'41.5"E, 18 m a.s.l.), which is positioned approximately 600 meters from

5 St. Peter's Basilica. This urban measurement site is surrounded by highly frequented streets,

6 separated from the courtyard by the four-storey building of the hospital. The surrounding area

7 is a touristic hotspot with frequent religious gatherings (e.g. festivals, masses) and many

8 restaurants and shops. Especially on Wednesdays during the papal audience and on Sundays,

9 if the masses are held at St. Peter's or during papal speeches (Angelus), the area attracts

10 numerous visitors.

11 The distance between the two measurement sites is around 17 km. During both years

12 measurements at Tor Vergata and central Rome were performed subsequently.

13

2.2 Instrumentation

15 All measurements were performed with the **Mo**bile aerosol research **La**boratory MoLa

16 (Drewnick et al., 2012). MoLa is based on a regular Ford Transit delivery vehicle equipped

17 with instruments for on-line measurements of chemical and physical properties of aerosols,

18 important trace gases and meteorological variables (Table 2). Further description as well as

19 details of the aerosol inlet system can be found in Drewnick et al. (2012). All results

20 presented in this study were obtained in stationary measurements, with the aerosol inlet and a

21 meteorological station at 7 m above ground level.

22 An HR-ToF-AMS (Aerodyne Research, Inc.; DeCarlo et al., 2006) was used to measure

23 particulate mass concentrations of submicron non-refractory organics ("Org"), sulphate

24 ("SO_4"), nitrate ("NO_3"), ammonium ("NH_4") and chloride ("Chl"). The HR-ToF-AMS

25 allows the distinction between different ions at the same nominal mass-to-charge-ratio (m/z).

26 The instrument was run in V-mode, i.e. the ions followed a "V"-shaped trajectory through the

27 mass spectrometer, allowing high sensitivity at slightly lower mass resolution, compared to

28 the higher resolution mode (W-mode).

29 In the framework of the EC-LIFE+ project DIAPASON additional measurements were

30 performed at the Tor Vergata measurement site, which aimed at assessing the contribution of

31 Saharan dust to PM levels. These measurements included hourly PM_{10}, a three-wavelength

Atmospheric
Chemistry
and Physics
Discussions

1   nephelometer, one-hour filter sampling for off-line PIXE analysis (Lucarelli et al., 2014) and

2   a polarization LIDAR-ceilometer for the assessment of presence, phase and altitude of aerosol

3   layers (Gobbi et al., 2004). Boundary layer heights were determined from polarisation

4   LIDAR-ceilometer measurements based on the method described by Angelini and Gobbi

5   (2014).

6   Since the POPE measurements were performed inside a courtyard, surrounded by four-storey

7   tall buildings, wind speed, wind direction and solar radiation data are affected and not used

8   for these periods. The time resolution for all measurements is 60 s or better.

9

10   **3   Data preparation and analysis**

11   **3.1   General data analysis**

12   All measured variables were corrected for sampling delays and set on a common 1-second

13   time base. Particle losses during the transport through the inlet system were negligible

14   (Drewnick et al., 2012). The data time series were carefully inspected and quality checked.

15   Data affected by instrument calibrations and malfunctions were removed. Measurement

16   periods influenced by local emissions (e.g. moving vehicles in the immediate vicinity of

17   MoLa) were identified based on prominent short peaks in the time series of CO_2 and particle

18   number concentration (PNC) which significantly exceeded the typical variability, and

19   removed from the data set. After data decontamination, 5-minute averages were calculated for

20   all variables, which were used for all following analyses if not otherwise indicated.

21   Data collected during the DIAPASON2013/POPE2013 and DIAPASON2014/POPE2014

22   field campaigns are presented in local winter (UTC+1) and local summer (UTC+2) time,

23   respectively. For convenience, DIAPASON2013 data are presented only in winter time, even

24   though the change from summer to winter time was at the fifth day of measurements

25   (27.10.2013). This means data measured prior to the time change is 1 hour shifted to the past

26   with respect to local (summer) time. Especially diurnal patterns dominated by anthropogenic

27   activity patterns (e.g. traffic during rush hour times) could be affected by ignoring the time

28   change. In order to evaluate this possible influence, diurnal cycles measured before and after

29   the time change were compared, but no significant shift of diurnal patterns was observed

30   between the time periods. Since diurnal cycles are not only modulated by the source emission

31   strengths, but also by boundary layer dynamics, we assume the missing evidence of the time

Atmospheric
Chemistry
and Physics
Discussions

1   shift in the data is caused by a combination of influence from boundary layer dynamics and

2   the temporal uncertainty of diurnal cycles calculated over only a few days. Additionally,

3   anthropogenic activities could have partially not been instantly adapted to the time change,

4   which would lead to a blurring of the effect of the time change on diurnal cycles.

5   Polar plots of species concentration as a function of local wind direction and wind speed were

6   generated by averaging species concentrations (60 s data) into bins of 5° wind direction and

7   0.5 m s^{-1} wind speed. The resulting data were smoothed by applying a natural neighbour

8   interpolation (Sibson, 1981). As presented by Yu et al. (2004), such polar plots can provide

9   directional information on sources in the vicinity of a monitoring site. Sources close to the

10   measurement site are typically indicated by concentration decreases with increasing wind

11   speed, while pollutants which are emitted from remote sources or at higher altitudes need

12   higher wind speeds to be transported to the monitoring site (Yu et al., 2004). Similarly,

13   Carslaw et al. (2006) reported the capability of such bivariate polar plots to distinguish

14   between no-buoyancy sources like traffic (decreased pollutant concentration with increasing

15   wind speed) and buoyant plumes emitted from sources like chimney stacks (increased

16   concentrations with increasing wind speed), where the plume needs to be brought down to

17   ground-level from a higher altitude.

18

19   3.2 HR-ToF-AMS data analysis

20   AMS data evaluation was performed within Igor Pro 6.37 (Wavemetrics) with the standard

21   AMS data analysis software SQUIRREL 1.55H and PIKA 1.14H. Elemental ratios calculated

22   from organic ion fragments (Aiken et al., 2007) were determined using APES light 1.06 (all

23   available at http://cires1.colorado.edu/jimenez-group/ToFAMSResources/ToFSoftware/). For

24   all data sets a collection efficiency of 0.5 was applied, which is typical for the given ambient

25   measurement conditions (Canagaratna et al., 2007). The ionisation efficiency (IE) of the ion

26   source and the relative ionisation efficiency (RIE) for ammonium and sulphate (e.g.

27   Canagaratna et al., 2007) were determined before the DIAPASON and after the POPE

28   campaigns in both years. An additional IE calibration in 2013 after the field measurements

29   showed no general trend in IE values. Therefore, the observed variability of the IE values is

30   assumed to stem only from the uncertainty of the calibrations, and for each year averages of

31   the determined IE and RIE values were used for data analysis. Measurements of particle free

1   air were carried out multiple times during the campaigns and were used for correction of

2   instrumental background effects.

3   In order to separate total OA into different aerosol types, PMF (Paatero and Tapper, 1994;

4   Ulbrich et al., 2009) was applied to high-resolution mass spectra of the OA fraction with *m/z*

5   below 131. The procedure of HR data and error matrices preparation is described in detail in

6   DeCarlo et al. (2010). Isotopes constrained to a fractional signal of their parent ion were

7   excluded from the analysis. Within the PMF Evaluation Tool v2.06 ions with signal-to-noise

8   ratio < 0.2 were removed from data and error matrices, and ions with signal-to-noise ratio

9   between 0.2 and 2 were down-weighted in the analysis by increasing their estimated error by

10   a factor of two (Ulbrich et al., 2009). Particulate CO_2^+ (*m/z* 44) and its associated ions at *m/z*

11   16, 17, 18 and 28 were down-weighted by a factor of $\sqrt{5}$ (Ulbrich et al., 2009, supplemental

12   information).

13   In order to find the most reasonable and robust PMF solution, the number of factors (one up

14   to ten, always at least two more than the finally selected solution), the rotational force

15   parameter (fPeak: -1 to 1; Δ = 0.1) and the starting point (seed: 0 to 50; Δ = 1) were varied

16   (see Ulbrich et al., 2009 for methodological details). Solutions with fPeak=0 and seed=0

17   turned out to yield robust results for all data sets. The evaluation of potential PMF solutions

18   was based on comparisons of the resulting factor time series with those of co-located

19   measurements (see Sect. 4.2), and of factor mass spectra with such from the literature.

20   Residues, i.e. the contribution of organic mass concentrations not included in any of the

21   factors, accounted for <1 % of the organics mass concentration in all used PMF solutions and

22   are therefore negligible.

23

4   Results and discussion

4.1   Overview: Differences between seasons and locations

26   This section provides a broad overview of the mean conditions of local meteorology and air

27   quality during each measurement campaign (Table 3, Fig. 1), and discusses their seasonal and

28   spatial differences. Figure 2 provides an overview of the relative composition of non-

29   refractory PM_1 plus BC and shows the contribution of different factors related to different

30   sources retrieved from the OA fraction using PMF. In total, seven different factors were

31   identified: OOA (oxygenated OA), SV-OOA (semi-volatile OOA), LV-OOA (low-volatile

Atmospheric
Chemistry
and Physics
Discussions

1   OOA), HOA (hydrocarbon-like OA), COA (cooking OA), BBOA (biomass burning OA) and

2   CSOA (cigarette smoke OA, see Sect. 4.2.5; considered local contamination and not included

3   in the pie charts in Fig. 2). Here, only a general overview of these different factors focusing on

4   seasonal and spatial differences is given. A more detailed discussion of the various sources

5   associated with these factors is provided in Sect. 4.2.

6   *Meteorology overview:*

7   The first period of the DIAPASON2013 campaign (23.-31.10.2013) was dominated by high

8   pressure influences and low wind speeds with air masses moving from the Atlantic across the

9   Mediterranean basin. Within this period dust from the Sahara was transported to the Rome

10   area (see Sect. 4.2.1). The second half of DIAPASON2013 (1.-7.11.2013) was characterized

11   by a pressure drop and increased wind speed together with some frontal passages leading to

12   precipitation. Both turbulent kinetic energy (TKE), which is a measure of the intensity of

13   turbulence and can be used as an indicator for the mixing efficiency of pollutants in the air

14   (Srivastava and Sarthi, 2002), and boundary layer heights (BLH) were at rather low levels

15   during DIAPASON2013 (Table 3), favouring the accumulation of pollutants.

16   The first measurement days of POPE2013 (07.-09.11.2013) were influenced by changing

17   weather conditions, followed by a low pressure system centred over Italy (10.-14.11.2013)

18   driving N-NW wind conditions and leading to almost daily precipitation events. High TKE

19   levels (almost three times higher compared to DIAPASON2013) and slightly increased

20   boundary layer heights (900 m compared to 850 m; Table 3) led to conditions were dilution of

21   pollutants was more favoured.

22   During DIAPASON2014 a low pressure system was located over the Atlantic and North

23   Africa. Saharan dust was advected to the measurement site during the first week of

24   measurements. Some precipitation events occurred during these advections. TKE was slightly

25   increased after the dust advection, favouring the reduction of pollutant concentrations.

26   Boundary layer heights reached around 1500 m (Table 3).

27   During POPE2014 a period of low pressure over the Atlantic and high pressure over Africa

28   and Europe (04.-13.6.2014) was followed by reversed conditions (14.-17.6.2014) with some

29   heavy precipitation events. Compared to DIAPASON2014 the boundary layer was slightly

30   higher (1560 m) and TKE was decreased by 20 %.

Atmospheric
Chemistry
and Physics
Discussions

1   During DIAPASON2013 local winds were predominantly arriving from south and south-

2   easterly directions, whereas during DIAPASON2014 south-westerly wind directions

3   dominated (Fig. 1; no data available for POPE2013/2014, see Sect. 2.2). No clear relationships

4   of air mass origin with measured PM_1 mass concentrations were found by the calculation of

5   HYSPLIT (Stein et al., 2015) and FLEXPART (Stohl et al., 2005) backward trajectories for

6   our measurement periods.

7   *Aerosols and trace gases:*

8   During both, Oct/Nov and May/June measurements, CO_2, NO_x and particulate PAH

9   concentrations (all typically traffic-related) were higher in central Rome compared to the

10   outskirt location (Table 3). Cooking-related aerosol (COA) concentrations were found to be

11   generally higher in the city centre (Fig. 2b, d), while traffic-related (HOA) concentrations

12   were strongly increased during 2014 (+ 58 %) at the urban location (Fig. 2d), and nearly the

13   same at both locations during the 2013 measurements (Fig. 2a, b). All this is consistent with

14   increased primary emissions (cooking, traffic) at the urban (Fig. 2b, d) compared to the

15   suburban site (Fig. 2a, c). However, total concentrations of organic aerosol predominantly of

16   primary origin (POA) were higher at the suburban (1.9-2.5 µg m^{-3}) compared to the urban

17   (1.4-1.6 µg m^{-3}) location. This is due to a factor indicating particles from biomass burning

18   (BBOA), which was obtained exclusively at Tor Vergata (Fig. 2a, c). Here, biomass burning

19   seems to be an important particle source, contributing the most abundant fraction (42-51 %)

20   of POA. Consistently, BC, which is related to primary emissions from both biomass burning

21   and traffic, showed no general trend between the two locations (Table 3).

22   The influence of increased temperatures and stronger solar radiation during measurements in

23   May/June 2014 (Table 3) is reflected in elevated ozone mixing ratios and the fact that it was

24   possible to extract an additional OOA factor, which was attributed to a fresher, less oxidised

25   aerosol type (SV-OOA, Fig. 2c, d). Within a continuum of OOA with different degrees of

26   aging/oxidation, SV-OOA (fresh, of rather local origin) and LV-OOA (aged, of more regional

27   origin) are located in the upper and lower range, respectively. In contrast, during Oct/Nov,

28   only one type of rather aged OOA was found (Fig. 2a, b), due to reduced photochemistry in

29   this season which prevents the quick formation of oxygenated aerosol from precursors emitted

30   in the vicinity.

31   A stronger influence of aged aerosol of rather regional origin on the PM_1 fraction was

32   observed for May/June than for Oct/Nov: the fraction of OOA (SV-OOA + LV-OOA) to OA,

1   but also the relative contribution of total organics and sulphate to PM_1 were higher in the

2   warmer season (Fig. 2c, d). This could be caused by different prevalent air mass origins,

3   though the analysis of backward trajectories provided no definite answers on this (see above).

4   Also the relative fraction of sulphate could be lowered in Oct/Nov due to an enhanced fraction

5   of primary particles as a consequence of lower boundary layer heights (Table 3) and,

6   potentially, higher emission strength of local sources during the colder season. Consistently,

7   in Oct/Nov 2013 at both measurement locations a higher BC fraction was observed compared

8   to May/June, and POA made up a larger fraction of the total measured organics (Fig. 2). Also

9   absolute BC concentrations were enhanced. Additionally, higher concentrations of NO_x and

10 PAH (increased by a factor of 3), and of total particle number concentration (PNC) were

11 observed during Oct/Nov (Table 3), indicating the accumulation of pollutants during the

12 colder season due to the aforementioned reasons.

13 *"Home-made" vs. "advected" PM_1:*

14 For a rough estimate of the contribution of PM_1 originating from sources in the Rome

15 metropolitan area and from advection from outside, PM_1 species were separated into "home-

16 made" (BC, HOA, COA, BBOA, SV-OOA, NO_3) and "advected" (OOA/LV-OOA, SO_4)

17 (Table 4). NH_4 was apportioned to home-made and advected PM_1 based on the molar

18 concentrations associated with NO_3 and SO_4, respectively. Not included in these estimates are

19 dust advection periods and emissions from cigarettes (which were considered as local

20 contaminations). During the measurements the fraction of home-made PM_1 accounted for 42-

21 70 % and advected PM_1 accounted for 30-58 % of total (home-made + advected) PM_1

22 (Table 4). During the 2013 measurements higher absolute concentrations of home-made PM_1

23 were found at the suburban location compared to the urban site, possibly caused by

24 meteorological conditions favouring pollutant accumulation during the respective period (see

25 above). During 2014, when meteorological conditions (e.g. BLH, TKE; see Table 3) were

26 rather comparable at both locations, similar absolute concentrations of home-made PM_1 were

27 observed at both sites. No general seasonal difference in home-made PM_1 fraction was

28 observed, although BLH was strongly increased during the May/June 2014 compared to the

29 Oct/Nov 2013 measurement periods. Partially, this might be due to the additional presence of

30 the home-made species SV-OOA during May/June, which could to some extent have

31 compensated for the dilution effect due to the increased BLH. Altogether, neither a general

32 spatial (DIAPASON vs. POPE) nor a seasonal (Oct/Nov vs. May/June) tendency regarding

33 the contribution of home-made and advected PM_1 to total PM_1 was observed. These results

Atmospheric
Chemistry
and Physics
Discussions

1   indicate that urban air quality in Rome strongly depends on both, emissions within the city

2   and transport of pollutants to the city, which both contribute to urban aerosol concentration.

3   Independent of measurement season and location the organics fraction always was found to

4   contribute the largest share of PM_1 (44-53 % of non-refractory PM_1 plus BC, Fig. 2), though

5   its relative composition (primary vs. secondary OA) differed. Regarding absolute PM_1

6   concentrations (Table 3 from EDM measurements, Fig. 2 from non-refractory components

7   plus BC) neither any general conclusion whether aerosol mass concentrations are higher at the

8   city centre or in the suburb, nor whether PM_1 concentrations are elevated during any of the

9   two different seasons, can be drawn. In the 2013 campaign total PM_1 mass concentrations

10   were more than doubled at the suburban compared to the urban location, whereas in the 2014

11   measurement PM_1 concentrations were increased by a factor of 1.4 at central Rome. As

12   discussed above, changes in meteorological conditions are likely one explanation for this

13   result: During DIAPASON2013 meteorological conditions favoured the accumulation of

14   pollutants, whereas the dilution of pollutants was favoured during the POPE2013

15   measurement period; during DIAPASON2014 and POPE2014 TKE and BLH were rather

16   similar leading to comparable pollutant dilution effects during the two measurement periods.

17   BLH were increased by around 75 % during May/June compared to Oct/Nov 2013, leading to

18   stronger dilution capacities in general. In addition to meteorological conditions (e.g. solar

19   radiation, BLH, TKE, air mass origin, etc.) local air quality can be strongly influenced by

20   local emission from various sources (traffic, cooking, biomass burning). A strong influence of

21   meteorological conditions (air mass origin) on air quality was also observed during the

22   MEGAPOLI campaign in Paris in July 2009, where variations in secondary aerosol

23   concentration mainly were attributed to such reasons (Freutel et al., 2013).

24

4.2   Aerosol sources: identification and characterisation

26   In this section the various aerosol types and sources which were identified from the data

27   obtained during the DIAPASON and POPE measurement campaigns in 2013 and 2014 are

28   discussed in more detail. Each identified aerosol type was characterized in an attempt to

29   determine its contribution to total particulate mass and its seasonal and spatial variability.

30   Furthermore, the potential origin of the identified aerosol types is discussed.

Atmospheric
Chemistry
and Physics
Discussions

1 4.2.1 Saharan dust

2   During each DIAPASON field campaign one dust advection event lasting for several days

3   was observed. The identification of the dust events with dust reaching down to the ground

4   was based on dust forecasts provided by the SKIRON model (Kallos et al., 1997) and on co-

5   located polarisation LIDAR-ceilometer measurements (Gian Paolo Gobbi, personal

6   communication). PIXE analysis of 1-hour filter samples confirmed a significant increase of

7   mineral dust concentrations at ground level during the identified dust periods (Silvia Nava,

8   personal communication 2016). Table 5 provides the time intervals of "dust" and "no dust"

9   (i.e. background with respect to dust advections) periods for DIAPASON2013 and

10   DIAPASON2014. Based on these, estimations regarding the contribution of dust to PM levels

11   were made by calculating the coarse particle fraction ($PM_{10-2.5}$) from EDM measurements for

12   the respective periods (Table 5).

13   During DIAPASON2013 a Saharan dust advection period was observed from October 29th

14   (5 pm) until November 1st (8 am) with $PM_{10-2.5}$ concentrations at ground level being increased

15   by 78 % with respect to background conditions. Total PM_{10} concentrations were elevated by

16   68 %, with 68 % and 70 % of mass belonging to PM_1 during the background and during the

17   dust event periods, respectively. This increase in absolute PM_1 with a slight increase in the

18   fraction of PM_1 during the dust advection compared to background conditions was also

19   reflected in the particle size distributions (Fig. 3, black traces). The dust event was forecasted

20   by the BSC-DREAM8b model (Basart et al., 2012; Perez et al., 2006a; Perez et al., 2006b)

21   and also HYSPLIT (Stein et al., 2015) back trajectories showed dust transport from the

22   Sahara with main dust sources located at 30-33N, between Morocco (Saharan Atlas) and SW

23   Tunisia (Erg Oriental), in the period 26.-28.10.2013, moving along an anti-cyclonic pattern.

24   During DIAPASON2014 a dust event was observed from May 20th (1 pm) until May 26th

25   (9 am). Here, the coarse particle fraction ($PM_{10-2.5}$) was increased by 180 % compared to the

26   "no dust" interval with much smaller fractions of particle mass in PM_1 (31 and 48 % in the

27   "dust" and "no dust" periods, respectively). The contribution of dust to the coarse particle

28   fraction with almost no contribution to the submicron fraction is reflected in the difference

29   particle mass size distribution (Fig. 3, bottom panel, red trace), which shows maximum mass

30   concentrations for aerodynamic particle diameters around 2 µm and smaller contributions

31   extending down to ~600 nm and up to more than 10 µm particle diameter. Comparing both

32   dust events in terms of particle sizes, the contribution of the dust advection event during

33   DIAPASON2014 was characterized by a broad particle mass size distribution with maximum

1 concentrations at particle sizes around 2 µm, whereas in 2013 two modes (with maxima

2 around 0.6 µm and 3 µm) were observed. Both the BSC-DREAM8b model and HYSPLIT

3 back trajectories showed dust transport from the Sahara to occur between 19.-22.05.2014

4 along a cyclonic pattern, with dust originating (as in October 2013) at 30-35N between

5 Morocco (Saharan Atlas) and SW Tunisia (Erg Oriental).

6 With regard to the coarse particle mode ($PM_{10-2.5}$) the dust event during DIAPASON2014 was

7 more distinct. In terms of absolute PM_{10} concentrations, higher concentrations at ground level

8 were reached during the dust advection measured during DIAPASON2013. However, with

9 respect to the "no dust" conditions, mean contributions of approximately 10 µg m^{-3} dust to

10 PM_{10} concentrations were observed during the campaigns in both years, which is lower than

11 the mean increase of PM_{10} in the order of 12-16 µg m^{-3} observed by Gobbi et al. (2013)

12 during dust advection events in the period 2001-2004. During both advection events legal

13 PM_{10} limits of the European Union (daily mean value of 50 µg m^{-3}) were not exceeded.

14 AMS data were investigated for potential impacts of Saharan dust advections on the chemical

15 composition of non-refractory submicron particles. Figure 4 presents the mean chemical

16 composition of non-refractory PM_1 measured during "dust" and "no dust" periods for both

17 DIAPASON campaigns. Only in 2013 minor differences in absolute mass concentrations

18 were observed, consistent with the slight increase of submicron particles observed in the mass

19 size distributions during this dust event (Fig. 3, bottom panel, black trace). However, the

20 relative composition remains the same for both periods in both years. This result suggests that

21 there was no significant influence of the dust advection on the chemical composition of the

22 submicron non-refractory aerosol fraction.

23 In order to cross-check whether differences in meteorological conditions could have biased

24 these results, and e.g. could have compensated for changes due to the dust affecting non-

25 refractory PM_1, averages of meteorological variables were calculated for "dust" and "no dust"

26 periods. The only slight differences found between dust events and background conditions

27 were in local wind directions (SE compared to S/SE in 2013, and SW compared to SSW in

28 2014) and (in 2013) in wind speeds ((1.4 ± 0.7) m s^{-1} compared to (2.0 ± 1) m s^{-1}). Since these

29 differences are only very minor, we conclude that our observation of comparable chemical

30 composition of non-refractory PM_1 during "dust" and "no dust" periods was not caused by

31 any compensating effects.

32

Atmospheric
Chemistry
and Physics
Discussions
Open Access
EGU

4.2.2 Secondary and aged aerosol: seasonal influence on formation processes and chemical composition

Seasonal variations of the characteristics of secondary and aged aerosols were identified by investigating new particle formation events and particle chemical composition measured during both POPE and DIAPASON campaigns in Oct/Nov 2013 and May/June 2014.

New particle formation:

Diurnal cycles of size-resolved and total particle number concentrations (PNC) for the Oct/Nov 2013 and May/June 2014 campaigns (Fig. 5) revealed several seasonal differences. During measurements in Oct/Nov 2013 (Fig. 5, left panels), elevated PNC were only observed during rush hour times in the morning and the evening, whereas in the measurements in May/June 2014, an additional PNC peak occurred with a maximum around 1-3 pm (DIAPASON2014) and 2-3 pm (POPE2014), respectively (Fig. 5, right panels). At the urban site (Fig. 5, bottom panels), PNC after the morning rush hour remain at an elevated level, likely because of increased background concentrations due to generally higher traffic density in the city centre. PNC were generally higher in the Oct/Nov 2013 than in the May/June 2014 campaigns, as discussed in Sect. 4.1.

Mean particle number size distributions for the period of maximum PNC at midday (Fig. 6; "nucleation"; solid traces) show a distinct mode at small particle diameters between 7-15 nm for both May/June 2014 campaigns (also visible in Fig. 5, right panels) compared to the number size distribution measured between 10-11 am (Fig. 6; "background"; dashed traces). Such occurrences of ultrafine particles at midday, when concentrations of particles from traffic are at a relative minimum and thus not responsible for strongly increased PNC, have been attributed before to new particle formation characteristic for urban areas with high solar radiation (Brines et al., 2015; Minguillon et al., 2015; Reche et al., 2011). During POPE2014 an additional mode at larger particle sizes (D_p approximately 15-50 nm) was found in the particle size distribution measured at midday (Fig. 6), probably originating from increased background levels.

During POPE2014 diurnal cycles of mean (grey) and median (black) PNC agree very well with each other, also during the midday peak (Fig. 5). This reflects the observed low day-to-day variability during this period for the measurements in central Rome, wherein the corresponding PNC time series a midday peak was observed on every single day. Local smoking activities (see Sect. 4.2.5) at the central Rome measurement location seem not to

Atmospheric
Chemistry
and Physics
Discussions

1   have biased these results, since no differences in diurnal cycles of PNC for weekdays

2   (smoking activities) and weekends (no smoking activities) have been found. This suggests

3   that the formation of new particles around midday was taking place every day at central Rome

4   during the May/June 2014 measurement period.

5   Conversely, the diurnal cycle of total PNC measured during DIAPASON2014 shows a clear

6   discrepancy between mean and median values during the midday peak (Fig. 5). This

7   discrepancy is due to the fact that new particle formation events did not occur on all days,

8   probably induced by different meteorological conditions and/or differences in pre-existing

9   particle surface areas (e.g. Kulmala and Kerminen, 2008).

10   To test whether particular meteorological conditions can promote/suppress new particle

11   formation events, "nucleation" and "non-nucleation" days were classified for

12   DIAPASON2014 by comparing PNC measured during 10-11 am (background conditions,

13   PNC_{bg}) and during 11 am - 4 pm (typical nucleation periods, PNC_{nuc}) (Table 6). This

14   classification was cross-checked by verifying if during classified nucleation days a clear

15   increase in PNC at small particle diameters ($D_p \leq 25$ nm) could be observed in the particle

16   number size distributions, and whether it was missing on classified non-nucleation days. Only

17   one potentially falsely classified nucleation day (24.05.2014) was found by checking these

18   criteria, and was moved to the class of non-defined days. The classification resulted in six

19   nucleation days, six non-defined days and two non-nucleation days.

20   Mean values for the time period 10 am to 4 pm (new particle formation period plus one

21   previous hour) were calculated for each day and averaged according to the above-mentioned

22   classification for the DIAPASON2014 campaign. Table 6 lists PNC of the classified periods

23   and variables potentially supporting new particle formation. A slight trend of increased

24   temperature, solar radiation and ozone levels and of low relative humidity characterizes

25   nucleation days compared to non-nucleation days and non-defined days. This is consistent

26   with previously reported association of high solar radiation (Pikridas et al., 2015; Shi et al.,

27   2001), low relative humidity (Kulmala and Kerminen, 2008) and increased ozone

28   concentrations (Harrison et al., 2000) with new particle formation events. No relationship

29   between the occurrence of new particle formation and the presence of Saharan dust was

30   observed. Different to the findings of Zhang et al. (2004), no increase of sulphate, ammonium

31   and nitrate concentrations was observed in our measurements during periods with new

32   particle formation events. Estimations based on the size distribution measurements during

33   DIAPASON2014 reveal that less than 1 % of PM_1 can be assigned to particles generated by

Atmospheric
Chemistry
and Physics
Discussions

Open Access

EGU

1   new particle formation. Therefore, it is not surprising that no significant influence of the

2   particle formation events on the AMS-measured chemical particle composition could be

3   observed.

4   In summary, our data do not provide sufficient statistical evidence to unequivocally determine

5   the driving factors for new particle formation. However, since indications for such were only

6   observed in the warmer season at both locations, it is probably linked to higher temperatures

7   and stronger solar radiation. Similar results were obtained from the MEGAPOLI

8   measurements in Paris, where new particle formation was only observed during summer

9   (Pikridas et al., 2015). During the May/June 2014 campaigns, new particle formation events

10 occurred roughly on 43 % of the measurement days at the suburban location, but on each

11 single day at central Rome, potentially due to increased concentrations of precursors and

12 higher prevailing mean temperatures (Table 3). In a long-term measurement study performed

13 by Costabile et al. (2010) the occurrence of aged nucleation mode particles (up to 30 nm) was

14 observed predominantly in spring in the area of Rome at a regional background site (located

15 more remotely than the Tor Vergata site) in the early afternoon (3 pm) when the measurement

16 site was located downwind of Rome (Brines et al., 2015). In contrast, during

17 DIAPASON2014 measurements, no dependency between nucleation events and wind

18 direction was observed, and the site was not located downwind of Rome during nucleation

19 periods. At this measurement location, probably less precursors are available than in central

20 Rome, but more precursors than at a remote regional background site such as in the study of

21 Costabile et al. (2010). This probably facilitates new particle formation events in the direct

22 vicinity of the site under favourable meteorological conditions, but independent of advection

23 of air masses from central Rome.

24 *Secondary and aged aerosol:*

25 Because of extremely low mass contributions from freshly formed particles to total particle

26 mass, new particle formation had no influence on the measured total organics mass

27 concentrations. However, a general seasonal difference in the composition of the oxygenated

28 organic aerosol (OOA) as determined in the PMF analysis was found, as discussed in the

29 following.

30 OOA, an aerosol type with increased oxygenation level, typically dominates the OA fraction.

31 It is assumed to be mainly formed in the atmosphere from gaseous biogenic and

32 anthropogenic precursors by photochemical oxidation, thus indicating SOA. Additionally,

Atmospheric
Chemistry
and Physics
Discussions

1   some OOA may originate from atmospheric aging of POA. Generally, aging processes are

2   reflected in an increased degree of aerosol oxidation (Jimenez et al., 2009) leading to a larger

3   fraction of m/z 44 (CO_2^+) in the aerosol mass spectra, generated by thermal decomposition of

4   carboxylic acids in the AMS (Ng et al., 2010). Additionally, a prominent peak in OOA mass

5   spectra occurs at m/z 43 ($C_3H_7^+$ and $C_2H_3O^+$). Under conditions where sufficient freshly

6   oxidised organic aerosol is available in the ambient air, PMF can separate the OOA into two

7   factors associated with mass spectra containing different relative fractions of m/z 44 and m/z

8   43 (f44 and f43, ratio of m/z 44 and m/z 43 signal, respectively, to the total signal of organics):

9   (I) A less oxidised, fresher, more locally produced semi-volatile OA (SV-OOA) associated

10 with higher f43, and (II) a stronger oxidised, more aged low-volatile OA (LV-OOA)

11 associated with higher f44 (Ng et al., 2010).

12 During our measurements the relative contribution of OOA to total organics varied between

13 42-76 %, with a slight increase during the warm period (Fig. 2). However, the main seasonal

14 difference was found in the composition of the OOA fraction. During the Oct/Nov 2013

15 campaign only one type of OOA was found, whereas for May/June 2014 PMF analysis

16 resulted in two OOA-factors: SV-OOA and LV-OOA. This observation is typical for

17 conditions with higher temperatures and stronger solar radiation, associated with increased

18 photochemistry (Jimenez et al., 2009), which enhance secondary aerosol formation and aging

19 processes and therefore facilitate the separation of OOA into fractions of different aging

20 levels. Similar observations were made during the MEGAPOLI measurements in Paris, where

21 only one factor describing OOA was identified in winter (Crippa et al., 2013a), whereas

22 during summer SV-OOA and LV-OOA could be separated (Crippa et al., 2013b).

23 The ratio of f44 to f43 gives an indication on the mean aging level of the aerosol (Fig. 7; Ng

24 et al., 2010). LV-OOA (from DIAPASON and POPE 2014, red markers) and OOA (from

25 DIAPASON and POPE 2013, green markers) fall into the same region in the f44 vs. f43 plot

26 (Fig. 7), indicating similar aging stages. SV-OOA (from DIAPASON and POPE 2014, blue

27 markers) shows a much higher fraction of m/z 43 together with a decreased m/z 44 fraction,

28 which suggests a low-oxidised, less aged particle type. Also the recombined "LV-OOA+SV-

29 OOA" (black markers in Fig. 7) shows a stronger contribution of f43 compared to OOA,

30 indicating an overall higher fraction of less oxidised organic aerosol in the warmer season.

31 We assume that LV-OOA (and OOA) is mainly advected and consists of strongly processed

32 material, whereas the low oxidation level of SV-OOA suggests a fresh, more locally produced

Atmospheric
Chemistry
and Physics
Discussions

1   aerosol which was quickly formed from regional precursors as a consequence of increased

2   photochemistry during this season.

3   This hypothesis is tested by the use of polar plots, which connect species concentration with

4   information on local wind direction and speed, thereby indicating the origin of a certain type

5   of aerosol (see Sect. 3.1). Figure 8a shows the colour coded concentration of SV-OOA, LV-

6   OOA, NO_3 and SO_4 depending on wind direction and speed obtained during the

7   DIAPASON2014 measurements. SV-OOA concentrations are increased during low wind

8   speed conditions, indicating nearby, no-buoyance sources. In contrast, LV-OOA

9   concentrations are almost independent of wind speed with only slightly increased

10   concentrations during periods of high wind speed with mainly south-westerly wind directions

11   (direction of Tyrrhenian Sea). This suggests that LV-OOA is not associated with sources

12   located in the vicinity of the measurement site, but long-range transported to the site e.g. over

13   the ocean or from central Europe. The polar plot characteristics of NO_3, which is often used as

14   a tracer for semi-volatile aerosol (DeCarlo et al., 2010; Lanz et al., 2007), show strong

15   similarities to the ones of SV-OOA (Fig. 8a). Also SO_4 and LV-OOA show polar plot patterns

16   similar to each other (Fig. 8a), confirming the characteristics of an aged, regionally

17   transported aerosol.

18   The polar plot of OOA obtained for DIAPASON2013 shows increased concentrations

19   particularly during periods of north-easterly, but also during south-westerly wind directions

20   (Fig. 8b). During conditions of low wind speed, OOA concentrations are increased

21   independent of the prevailing wind direction. In contrast to the findings for DIAPASON2014,

22   for this data set similar polar plot characteristics as for OOA were observed partly in the plots

23   of NO_3, NH_4 and SO_4 (Fig. 8b). Elevated NH_4 and SO_4 concentrations were mainly measured

24   during times with south-westerly wind direction, whereas NO_3 was rather advected from

25   north-easterly direction. Based on the polar plot characteristics no consistent trend indicating

26   the aging level, the source or the formation process of the OOA fraction can be observed,

27   consistent with the assumption of advection of a rather aged type of OOA together with

28   different amounts of NO_3, SO_4 and NH_4 depending on air mass history.

29

30   **4.2.3 Particles from biomass burning**

31   The type of primary organic aerosol at Tor Vergata identified from PMF analysis which had

32   the largest share during both measurement periods was attributed to biomass burning

Atmospheric
Chemistry
and Physics
Discussions

1 (biomass burning OA, BBOA). BBOA was identified by comparison with the time series of

2 known ion fragments of levoglucosan ($C_3H_5O_2^+$ (*m/z* 73) and $C_2H_4O_2^+$ (*m/z* 60); Schneider et

3 al., 2006) and by correlating the BBOA mass spectra with those presented by Mohr et al.

4 (2012). With Pearson's R^2 = 0.57-0.59 rather poor correlations were obtained, which

5 demonstrates the complexity and the potential variations of the BBOA mass spectra due to

6 aging processes and differences in source processes (e.g. different burning conditions or fuels;

7 Weimer et al., 2008). The mean BBOA mass concentration was 1.28 µg m^{-3} (24 % of total

8 OA) during Oct/Nov 2013 and 0.82 µg m^{-3} (18 % of total OA) during May/June 2014,

9 respectively (Fig. 2). Increased BBOA concentrations during the colder season probably result

10 from stronger agricultural burning activities (green waste burning) and domestic heating, as

11 well as from lower boundary layer heights. In the evening of 25.10.2013 during a strong,

12 visually detectable biomass burning event, which could be related to green waste burning in

13 the nearby Alban Hills, maximum concentrations of BBOA were obtained (up to 75 µg m^{-3}).

14 This event was used during the identification of the PMF solution: Only a factor including this

15 event could be considered to be attributed to biomass burning emissions.

16 The origin of BBOA emissions was further investigated by relating BBOA mass

17 concentrations to local wind direction and speed (see Sect. 3.1). The resulting polar plots (Fig.

18 9) indicate BBOA particles mainly arriving from south-easterly directions during

19 DIAPASON2013. During this measurement period agricultural fires were frequently observed

20 in the Alban Hills (Frascati vineyard area), which are located in this direction. Additionally,

21 BBOA was observed during conditions of north-easterly winds and higher wind speeds (up to

22 4 m s^{-1}), possibly resulting from residential wood burning in a densely populated urban

23 periphery area (Borghesiana). The polar plot of BBOA obtained from DIAPASON2014

24 measurements does hardly point to any preferential direction of BBOA origin. Since elevated

25 BBOA concentrations were mainly reached during low wind speed conditions, emission from

26 rather local sources is suggested.

27 BBOA was not identified in the measurements in the city centre of Rome, even not in PMF

28 solutions with a large number of factors (8). Since green-waste burning and domestic heating

29 with biomass are forbidden in central Rome, biomass burning related particles are probably

30 not emitted in the local environment. However, the contribution of biomass burning and

31 domestic heating to the urban air pollution of Rome (especially during winter time) was

32 reported by Gariazzo et al. (2016). Apparently, during our measurements in late spring and

33 autumn the contribution of particles emitted outside the suburban area is too small to be

1   identified with PMF and/or aging processes during the transport of the particles lead to a loss

2   of the BBOA fingerprint (Bougiatioti et al., 2014). Also during the MEGAPOLI

3   measurements in Paris emissions from biomass burning were identified in the organic aerosol

4   fraction (Crippa et al., 2013a). In contrast to our measurements, in Paris BBOA was only

5   found during the winter time campaign (Jan/Feb), but also at the measurement location in the

6   city centre, probably generated by local domestic wood burning (Crippa et al., 2013a).

7   In summary, the results from both DIAPASON measurements show that particles from

8   biomass burning significantly (18 – 24 % of total OA) contributed to local air pollution in the

9   suburban area in late autumn as well as in late spring. Agricultural fires and possibly wild

10   fires probably are their most important sources, since heating activities are assumed to be

11   quite low at these times due to the moderate temperature conditions (Table 3).

12

4.2.4   Emissions related to traffic and cooking activities

14   At both measurement locations, during both seasons particles from traffic- as well as from

15   cooking-related emissions were detected.

16   Indications of traffic-related emissions can be found in several measured variables showing a

17   distinct diurnal pattern with peaks during the morning and evening rush hours. The time series

18   and diurnal pattern of HOA (hydrocarbon-like organic aerosol), a PMF factor that is typically

19   associated with traffic emissions, show good agreement with the respective patterns of species

20   like BC, NO_x and PAH (diurnal cycles: $R^2 > 0.85$) for all four campaigns. Also correlations of

21   complete campaign time series of HOA with BC result in good agreements ($R^2 \approx 0.7$).

22   In the diurnal cycles of HOA seasonal and spatial differences can be observed (Fig. 10).

23   Independent of season and measurement location a short peak occurs during the morning rush

24   hour and a broader peak starting during the evening rush hour. During all field campaigns

25   except DIAPASON2013, HOA concentrations remain increased throughout the night. Thus,

26   the exact period of the evening rush hour cannot be clearly isolated. These differences in the

27   shapes of the HOA peaks in the morning and evening rush hour are mainly controlled by

28   boundary layer dynamics together with the diurnal cycle of traffic-related emissions (rush

29   hour times). A seasonal difference is observed in the HOA evening rush hour peak, which

30   peaks around midnight during May/June, but around 7-8 pm during Oct/Nov. This shift and

1   the broadening of the HOA peak in May/June 2014 is probably driven by the different

2   boundary layer dynamics during the two seasons.

3   For both measurement years a time shift of the morning peak between Tor Vergata and central

4   Rome (later by about one hour) can be observed. Since similar diurnal temperature profiles

5   measured at the suburban and the urban location suggest also similar boundary layer

6   dynamics at the two sites, the observed shift possibly results because traffic starts in the

7   suburbs earlier in the morning and continues slowly towards the city centre. In contrast to our

8   observations, from BC measurements during the MEGAPOLI summer campaign in Paris no

9   distinct shift of the morning rush hour peak was observed between the two suburban and the

10 urban measurement locations (Freutel et al., 2013).

11 Mean HOA mass concentrations for the individual measurement campaigns range between

12 0.59 - 0.93 µg m^{-3}. During the 2013 measurements (Oct/Nov) similar concentrations were

13 obtained at the suburban site (0.76 ± 1.04 µg m^{-3}) and central Rome (0.71 ± 0.72 µg m^{-3}),

14 whereas in 2014 higher concentrations were reached at central Rome (0.93 ± 0.73 µg m^{-3})

15 compared to the suburb (0.59 ± 0.60 µg m^{-3}). Overall, the contribution of traffic-related

16 emissions (e.g. HOA, NO$_x$, PAH) to local air pollutant levels was higher in central Rome, as

17 already discussed in Sect. 4.1.

18 A factor associated with cooking emissions, COA (cooking OA), was obtained by PMF

19 analysis of the OA measured at both locations and during both seasons. The COA mass

20 spectra show prominent peaks at *m/z* 41 and 55 (Allan et al., 2010; Lanz et al., 2007) and a

21 smaller contribution of *m/z* 60 and 73 (Mohr et al., 2009). Our COA mass spectra correlated

22 well with those found by Faber et al. (2013) and Mohr et al. (2012) with $R^2 = 0.63$-0.93.

23 The COA diurnal cycles observed at central Rome (Fig. 11, upper panel) are consistent with

24 results from previous studies (e.g. Allan et al., 2010; Mohr et al., 2012) showing highest

25 concentrations in the late evening (around 10 pm) and a smaller peak around midday (2-3

26 pm). This pattern is generated by a combination of source strengths and boundary layer

27 dynamics, with typically increased boundary layer height during lunch time compared to

28 dinner time.

29 In contrast, diurnal cycles of the COA factors measured at the suburban location in 2013 and

30 2014 (Fig. 11, lower panel) both show a peak in the evening, but only during

31 DIAPASON2014 a slight and barely significant COA concentration increase was observed

32 during lunch time. This could be due to an insufficient separation of the COA and HOA factor

1   during PMF analysis, which is also demonstrated in the COA "morning peak" of the

2   DIAPASON2014 measurements. However, the missing midday peak also reflects the

3   generally low abundance of cooking-related OA at the suburban measurement location: while

4   there are strong cooking activities and a large abundance and closeness of restaurants around

5   the central Rome site, potential sources in the immediate vicinity of the suburban site are

6   scarce. At a distance of around 250 m from our monitoring site, a cafeteria served hot meals

7   for lunch, but apparently, our measurements were not strongly affected by its emissions.

8   Consistently, absolute mass concentrations of cooking-related emissions were higher at the

9   central Rome site (0.70 ± 1.00 µg m^{-3}, 0.65 ± 0.69 µg m^{-3} in 2013 and 2014, respectively)

10 compared to the suburban measurement location (0.45 ± 0.50 µg m^{-3}, 0.53 ± 1.29 µg m^{-3}).

11 Ranging between 8-29 % of the total OA concentrations, cooking activities contribute

12 significantly to (sub-) urban air pollution. During meal times the contribution of COA to total

13 organics can be very high: For example during lunch/dinner times at central Rome, COA

14 contribution to total organics was 35 %/53 % (POPE2013) and 9 %/25 % (POPE2014),

15 respectively. Similar observations were made during the MEGAPOLI winter measurements in

16 Paris, where COA contributed on average 11-17 % to total OA (up to 35 % during lunch

17 times) (Crippa et al., 2013a).

18

19 **4.2.5 Cigarette smoking emissions**

20 For both POPE campaigns in central Rome PMF analysis of the organic aerosol fraction

21 resulted in a factor which could be associated with cigarette smoke (CSOA; excluded from

22 Fig. 2). This was not very surprising, since cigarette smoking took place in the direct vicinity

23 of the measurement location. The mass spectra of CSOA from both years show good

24 correlation with each other (R^2 = 0.7; Fig. 12). Very characteristic for the CSOA spectra is a

25 peak at m/z 84 from $C_5H_{10}N^+$ (Fig. 12). This ion (*N*-methylpyrrolidine) is typically observed

26 in EI mass spectra of nicotine (NIST: http://webbook.nist.gov, last access 09.05.2016) and is

27 generated by cleavage of the nicotine molecule into two heterocycles (Jacob III and Byrd,

28 1999). Since nicotine is one of the most abundant particulate compounds identified in

29 cigarette smoke samples (Rogge et al., 1994), its fragments are suitable tracers for cigarette

30 emissions. While cigarette smoke-related aerosol has been found in AMS measurements

31 previously (Faber et al., 2013; Fröhlich et al., 2015) and also the detection of nicotine from

32 cigarette smoke was mentioned (Jayne et al., 2000), to our knowledge, the identification of

1   the nicotine fragment *N*-methylpyrrolidine from analysis of HR-ToF-AMS data is reported

2   here for the first time. The time series of $C_5H_{10}N^+$ was used during the evaluation of the PMF

3   results as tracer for CSOA, yielding good correlations ($R^2 > 0.9$) with the time series of

4   CSOA.

5   The CSOA mass spectra from both POPE campaigns show reasonable to very good

6   agreement with CSOA mass spectra reported by Faber et al. (2013) ($0.65 < R^2 < 0.96$). Some

7   differences are observed between the mass spectra obtained for POPE2013 and 2014 in the

8   relative fraction of CO_2^+ and its related ions, which also affects the observed elemental ratios

9   (Fig. 12). This results in a potential error in CSOA concentrations of less than 10 % and

10   probably is due to a PMF artefact and/or insufficient correction for gas phase CO_2.

11   Comparison with mass spectra of cigarette smoke obtained in the laboratory (Faber et al.,

12   2013) show a contribution of CO_2^+ more similar to the POPE2013 measurements. Further

13   laboratory work in order to obtain more robust source spectra is needed to better constrain the

14   expected f44 in CSOA mass spectra. Due to the low intensity of the N-containing ions and a

15   conservative selection of ions which were fitted in the mass spectra reported by Faber et al.

16   (2013), the nicotine fragment ($C_5H_{10}N^+$) was not observed in their measurements of cigarette

17   smoke. However, after re-analysis of the mass spectra with integration of the $C_5H_{10}N^+$ ion in

18   the fitting procedure, a contribution of the nicotine tracer ion is clearly visible (Peter Faber,

19   personal communication).

20   Also the time series of mass concentration of the CSOA factor clearly support its attribution

21   to cigarette smoking emissions. The diurnal cycle of the CSOA factor strongly correlates with

22   typical working hours at the measurement location and with the diurnal cycle of the marker

23   fragment $C_5H_{10}N^+$ ($R^2 = 0.98$ for POPE2013 and POPE2014), exemplarily shown for

24   POPE2014 in Fig. 13 (top). Averaged CSOA mass concentrations for each day of the week

25   (Fig. 13; bottom) show distinct differences between working days and weekend, when the

26   administration of the hospital where the measurements took place was closed, supporting the

27   attribution of this PMF factor to locally emitted CSOA. Very similar observations were made

28   during the POPE2013 measurements.

29   Particles from cigarette smoke contributed 9-24 % (0.62-0.76 µg m^{-3}) to the total organic

30   aerosol mass measured at the location in central Rome. No indications for cigarette emissions

31   were found during the DIAPASON measurements. This result shows a potentially strong

32   influence on air quality in the direct environment of smokers, like it was also observed by

33   Faber et al. (2013) and Fröhlich et al. (2015). Since in our measurement, CSOA is mostly

**Atmospheric
Chemistry
and Physics**
Discussions

1   produced close to the measurement location (i.e., can be regarded a local contamination), it

2   was not included in the previous analyses of organic aerosol composition (see Sect 4.1).

3   *$C_5H_{10}N^+$ as a potential CSOA marker ion:* The ion $C_5H_{10}N^+$ was further investigated in order

4   to assess its applicability and limitations as a tracer for cigarette emissions in AMS data sets.

5   While the nicotine fragment ion $C_5H_{10}N^+$ (*m/z* 84.08) seems to be unique to cigarette

6   emissions, the proximity of the ions $C_5H_8O^+$ (*m/z* 84.06) and $C_6H_{12}^+$ (*m/z* 84.09) in the mass

7   spectra causes interferences, since the mass resolution of the instrument (R ≈ 2000 in V-

8   mode) is not sufficient for completely separating the individual ion signals. Mass spectra of

9   the primary organic aerosol PMF factors (HOA, COA, BBOA) which are not related to

10   cigarette emissions ("POA_{noCSOA}") show significant contributions (0.2 to 0.7 % of total

11   organics mass spectral signal) of the ions $C_5H_8O^+$ and $C_6H_{12}^+$, leading to an artificial increase

12   of the nicotine tracer ion signal. In contrast, for OOA mass spectra the contribution of these

13   ions is comparatively low (0.1 % of total organics mass spectral signal), which is why a

14   potential interference of OOA was neglected in the following considerations.

15   AMS measurements performed during DIAPASON2013 and DIAPASON2014, which are

16   assumed to be not influenced by local cigarette emissions, were used to quantify the

17   concentration-dependent influence of POA_{noCSOA} on the nicotine tracer ion $C_5H_{10}N^+$ due to

18   fitting interferences from the neighbour ions $C_5H_8O^+$ and $C_6H_{12}^+$. A linear relationship

19   between $C_5H_{10}N^+$ and POA_{noCSOA} was observed for a POA_{noCSOA} concentration range of 0-10

20   µg m^{-3}. Using the mass contribution of $C_5H_{10}N^+$ to the total CSOA mass spectra (Fig. 12;

21   1.8 % and 1.9 % for POPE2013/2014, respectively), the corresponding ion signals were

22   converted into CSOA detection limits. It was found that, under conservative considerations,

23   CSOA concentrations of at least 10 % of POA_{noCSOA} are needed in order to exceed detection

24   limits. During conditions of negligible POA_{noCSOA} concentrations, a CSOA detection limit of

25   80 ng m^{-3} was estimated.

26   Based on these estimations, it can be concluded that $C_5H_{10}N^+$ is a suitable nicotine tracer ion

27   for HR-AMS measurements which are influenced by local cigarette emissions (i.e., CSOA

28   larger than 10 % of POA_{noCSOA}) and can be used to estimate CSOA concentrations or to

29   identify a CSOA factor from PMF analysis. Urban background concentrations of cigarette-

30   related particles in the range of 1 % of PM_1, as reported by Rogge et al. (1994), however, are

31   below the estimated CSOA detection limits. This is still true when considering typical

32   contributions of OOA to total organics (~50 %) and of OA to PM_1 (also ~50 %), leading to a

33   CSOA detection limit of around 2.5 % of PM_1. In order to identify cigarette smoke

1   contributions in the order of 1 % of PM_1, higher mass spectral resolution is needed to be able

2   to separate the nicotine tracer ion from its neighbouring ions. Nevertheless, the fitting of

3    $C_5H_{10}N^+$ at m/z 84 could be worthwhile for HR-AMS data sets which are potentially

4   influenced by cigarette-related particles. In future work, it should be investigated how aging

5   processes affect the appearance of this marker ion in the mass spectra.

6

5   Summary and conclusions

8   Intensive field campaigns have been performed during Oct/Nov 2013 and May/June 2014,

9   each time consecutively at two locations (suburban, urban) in the area of Rome, enabling the

10   study of seasonal and spatial differences of aerosol and trace gas characteristics.

11   During both years at the suburban location an impact of advected Saharan dust on PM_{10} levels

12   was detected. With respect to background conditions, increases of PM_{10} by 68 % (2013) and

13   100 % (2014) were measured, corresponding to average absolute increases of about 10 µg

14   m^{-3}. No influence of the dust occurrence on the non-refractory PM_1 chemical composition was

15   found during the advections.

16   At both locations, during the Oct/Nov measurements air quality was more strongly influenced

17   by primary emissions (e.g. BC, NO_x, PAH) with generally increased particle number

18   concentration (PNC), whereas during May/June the contribution from secondary particles

19   (sulphate, aged OA) and ozone was more important. Also during May/June 2014, new particle

20   formation was frequently detected around midday, while in the colder season no distinct

21   increase of PNC took place outside typical rush hour times. The consequence of higher

22   temperatures plus stronger solar radiation was also visible in the SOA-related fraction of the

23   organic aerosol: During the warmer season two types of OOA (less oxidised, fresher SV-

24   OOA and strongly oxidised, older LV-OOA) were identified, while during the colder season

25   only strongly oxidised OOA was found.

26   Typical tracers for anthropogenic emissions (CO_2, NO_x, PAH, HOA, COA) were increased at

27   the urban measurement location. However, absolute concentrations of POA were higher at the

28   suburban location, due to a strong contribution from biomass burning OA, which here

29   accounted for 1.28 µg m^{-3} (24 % of total OA) and for 0.82 µg m^{-3} (18 % of total OA) in

30   Oct/Nov 2013 and May/June 2014, respectively. To a large degree this was related to

31   agricultural waste burning in the surrounding areas and during Oct/Nov2013 potentially also

32   to residential wood burning in the urban periphery.

Atmospheric
Chemistry
and Physics
Discussions

1   Cooking- and traffic-related aerosol was observed at both locations during both seasons. The

2   diurnal cycles of HOA (traffic-related OA) always peaked during rush hour times. A time

3   shift in the morning rush hour peak between the suburban site and central Rome was

4   observed, likely as a consequence of traffic progressing from the suburbs to the city centre.

5   HOA accounted for 0.59 to 0.93 µg m^{-3} (13 to 29 % of OA) at the different locations and

6   seasons. COA, as an indicator for cooking activities, showed maximum concentrations during

7   lunch and dinner times at central Rome, whereas at the suburban location only during dinner

8   times distinct peaks were observed. Average COA mass concentrations of 0.45 to 0.70 µg m^{-3}

9   (8 to 29 % of OA) were found, with higher concentrations observed at central Rome

10   compared to the suburban location (2013: +50 %; 2014: +23 %), as expected due to the higher

11   density of related sources.

12   A type of OA related to nearby cigarette emissions (CSOA) was detected at central Rome,

13   and found to strongly correlate with a characteristic nicotine fragment (N-methylpyrrolidine,

14   $C_5H_{10}N^+$) at m/z 84 in the mass spectra. This ion could serve as a suitable tracer for locally

15   emitted cigarette smoke also for other datasets. However, in order to identify CSOA based

16   solely on this tracer ion, CSOA must account for at least 10 % of the sum of COA, HOA and

17   BBOA, due to interferences of neighbouring ion signals from these POA types. In the absence

18   of those, a detection limit of 80 ng m^{-3} was found for CSOA. These findings imply that the

19   resolution of the HR-AMS is not sufficient to identify urban background contributions of

20   cigarette emissions (~1 % of PM$_1$, Rogge et al., 1994) based solely on $C_5H_{10}N^+$, while fitting

21   of this ion could be worthwhile for HR-AMS datasets which are potentially influenced by

22   nearby cigarette emissions.

23   During our measurements sub-micron aerosol originating from sources in the metropolitan

24   area of Rome and particles being advected from outside (dust periods were excluded)

25   contributed 42-70 % and 30-58 % to total measured PM$_1$, respectively. Thus, during our

26   measurements approximately half of the locally measured PM$_1$ was "home-made".

27   While for individual aerosol types clear spatial and temporal characteristics were observed

28   and can be understood, no general conclusion can be drawn whether total aerosol mass

29   concentrations are generally higher at the suburb or the city centre. Instead, consistent with

30   observations made in the area of Paris (Freutel et al., 2013), it was found that aerosol levels

31   strongly depend on the combination of meteorological conditions (e.g. origin of air masses,

32   dilution capacity within the boundary layer) and contributions of secondary aerosols and local

33   emissions.

Atmospheric
Chemistry
and Physics
Discussions

Open Access

EGU

9

10 **References**

11 Aiken, A. C., DeCarlo, P. F., and Jimenez, J. L.: Elemental analysis of organic species with

12 electron ionization high-resolution mass spectrometry, Analytical Chemistry, 79, 8350-8358,

13 2007.

14 Alam, A., Shi, J. P., and Harrison, R. M.: Observations of new particle formation in urban air,

15 J. Geophys. Res.-Atmos., 108, 2003.

16 Allan, J. D., Williams, P. I., Morgan, W. T., Martin, C. L., Flynn, M. J., Lee, J., Nemitz, E.,

17 Phillips, G. J., Gallagher, M. W., and Coe, H.: Contributions from transport, solid fuel

18 burning and cooking to primary organic aerosols in two UK cities, Atmos. Chem. Phys., 10,

19 647-668, 2010.

20 Alpert, P., Krichak, S. O., Tsidulko, M., Shafir, H., and Joseph, J. H.: A dust prediction

21 system with TOMS initialization, Monthly Weather Review, 130, 2335-2345, 2002.

22 Angelini, F. and Gobbi, G. P.: Some remarks about lidar data preprocessing and different

23 implementations of the gradient method for determining the aerosol layers, Annals of

24 Geophysics, 57, 2014.

25 Barnaba, F. and Gobbi, G. P.: Aerosol seasonal variability over the Mediterranean region and

26 relative impact of maritime, continental and Saharan dust particles over the basin from

27 MODIS data in the year 2001, Atmos. Chem. Phys., 4, 2367–2391, 2004.

28 Basart, S., Perez, C., Nickovic, S., Cuevas, E., and Maria Baldasano, J.: Development and

29 evaluation of the BSC-DREAM8b dust regional model over Northern Africa, the

30 Mediterranean and the Middle East, Tellus Ser. B-Chem. Phys. Meteorol., 64, 2012.

31 Boucher, O., Randall, D., Artaxo, P., Bretherton, C., Feingold, G., Forster, P., Kerminen, V.-

32 M., Kondo, Y., Liao, H., Lohmann, U., Rasch, P., Satheesh, S. K., Sherwood, S., Stevens, B.,

Atmospheric
Chemistry
and Physics
Discussions

1 and Zhang, X. Y.: 2013: Clouds and Aerosols. In: Climate Change 2013: The Physical

2 Science Basis. Contribution of Working Group I to the Fifth Assessment Report of the

3 Intergovernmental Panel on Climate Change, Cambridge, United Kingdom and New York,

4 NY, USA, 2013.

5 Bougiatioti, A., Stavroulas, I., Kostenidou, E., Zarmpas, P., Theodosi, C., Kouvarakis, G.,

6 Canonaco, F., Prévôt, A. S. H., Nenes, A., Pandis, S. N., and Mihalopoulos, N.: Processing of

7 biomass-burning aerosol in the eastern Mediterranean during summertime, Atmos. Chem.

8 Phys., 14, 4793-4807, 2014.

9 Brines, M., Dall'Osto, M., Beddows, D. C. S., Harrison, R. M., Gomez-Moreno, F., Nunez,

10 L., Artinano, B., Costabile, F., Gobbi, G. P., Salimi, F., Morawska, L., Sioutas, C., and

11 Querol, X.: Traffic and nucleation events as main sources of ultrafine particles in high-

12 insolation developed world cities, Atmos. Chem. Phys., 15, 5929-5945, 2015.

13 Canagaratna, M. R., Jayne, J. T., Jimenez, J. L., Allan, J. D., Alfarra, M. R., Zhang, Q.,

14 Onasch, T. B., Drewnick, F., Coe, H., Middlebrook, A., Delia, A., Williams, L. R., Trimborn,

15 A. M., Northway, M. J., DeCarlo, P. F., Kolb, C. E., Davidovits, P., and Worsnop, D. R.:

16 Chemical and microphysical characterization of ambient aerosols with the aerodyne aerosol

17 mass spectrometer, Mass Spectrometry Reviews, 26, 185-222, 2007.

18 Carslaw, D. C., Beevers, S. D., Ropkins, K., and Bell, M. C.: Detecting and quantifying

19 aircraft and other on-airport contributions to ambient nitrogen oxides in the vicinity of a large

20 international airport, Atmos. Environ., 40, 5424-5434, 2006.

21 Costabile, F., Amoroso, A., and Wang, F.: Sub-µm particle size distributions in a suburban

22 Mediterranean area. Aerosol populations and their possible relationship with HONO mixing

23 ratios, Atmos. Environ., 44, 5258-5268, 2010.

24 Crippa, M., DeCarlo, P. F., Slowik, J. G., Mohr, C., Heringa, M. F., Chirico, R., Poulain, L.,

25 Freutel, F., Sciare, J., Cozic, J., Di Marco, C. F., Elsasser, M., Nicolas, J. B., Marchand, N.,

26 Abidi, E., Wiedensohler, A., Drewnick, F., Schneider, J., Borrmann, S., Nemitz, E.,

27 Zimmermann, R., Jaffrezo, J. L., Prevot, A. S. H., and Baltensperger, U.: Wintertime aerosol

28 chemical composition and source apportionment of the organic fraction in the metropolitan

29 area of Paris, Atmos. Chem. Phys., 13, 961-981, 2013a.

30 Crippa, M., El Haddad, I., Slowik, J. G., DeCarlo, P. F., Mohr, C., Heringa, M. F., Chirico,

31 R., Marchand, N., Sciare, J., Baltensperger, U., and Prevot, A. S. H.: Identification of marine

32 and continental aerosol sources in Paris using high resolution aerosol mass spectrometry, J.

33 Geophys. Res.-Atmos., 118, 1950-1963, 2013b.

Atmospheric
Chemistry
and Physics
Discussions

Open Access

1   DeCarlo, P. F., Kimmel, J. R., Trimborn, A., Northway, M. J., Jayne, J. T., Aiken, A. C.,

2   Gonin, M., Fuhrer, K., Horvath, T., Docherty, K. S., Worsnop, D. R., and Jimenez, J. L.:

3   Field-Deployable, High-Resolution, Time-of-Flight Aerosol Mass Spectrometer, Analytical

4   Chemistry, 78, 8281-8289, 2006.

5   DeCarlo, P. F., Ulbrich, I. M., Crounse, J., de Foy, B., Dunlea, E. J., Aiken, A. C., Knapp, D.,

6   Weinheimer, A. J., Campos, T., Wennberg, P. O., and Jimenez, J. L.: Investigation of the

7   sources and processing of organic aerosol over the Central Mexican Plateau from aircraft

8   measurements during MILAGRO, Atmos. Chem. Phys., 10, 5257-5280, 2010.

9   DIAPASON: available at: http://www.diapason-

10   life.eu/index.php?option=com_content&view=article&id=171&Itemid=466&lang=en, last

11   access: 13.07.2016.

12   Drewnick, F., Boettger, T., von der Weiden-Reinmueller, S. L., Zorn, S. R., Klimach, T.,

13   Schneider, J., and Borrmann, S.: Design of a mobile aerosol research laboratory and data

14   processing tools for effective stationary and mobile field measurements, Atmospheric

15   Measurement Techniques, 5, 1443-1457, 2012.

16   Faber, P., Drewnick, F., Veres, P. R., Williams, J., and Borrmann, S.: Anthropogenic sources

17   of aerosol particles in a football stadium: Real-time characterization of emissions from

18   cigarette smoking, cooking, hand flares, and color smoke bombs by high-resolution aerosol

19   mass spectrometry, Atmos. Environ., 77, 1043-1051, 2013.

20   Freutel, F., Schneider, J., Drewnick, F., von der Weiden-Reinmuller, S. L., Crippa, M.,

21   Prevot, A. S. H., Baltensperger, U., Poulain, L., Wiedensohler, A., Sciare, J., Sarda-Esteve,

22   R., Burkhart, J. F., Eckhardt, S., Stohl, A., Gros, V., Colomb, A., Michoud, V., Doussin, J. F.,

23   Borbon, A., Haeffelin, M., Morille, Y., Beekmann, M., and Borrmann, S.: Aerosol particle

24   measurements at three stationary sites in the megacity of Paris during summer 2009:

25   meteorology and air mass origin dominate aerosol particle composition and size distribution,

26   Atmos. Chem. Phys., 13, 933-959, 2013.

27   Fröhlich, R., Cubison, M. J., Slowik, J. G., Bukowiecki, N., Canonaco, F., Croteau, P. L.,

28   Gysel, M., Henne, S., Herrmann, E., Jayne, J. T., Steinbacher, M., Worsnop, D. R.,

29   Baltensperger, U., and Prévôt, A. S. H.: Fourteen months of on-line measurements of the non-

30   refractory submicron aerosol at the Jungfraujoch (3580 m a.s.l.) – chemical composition,

31   origins and organic aerosol sources, Atmos. Chem. Phys., 15, 11373-11398, 2015.

32   Fuller, G. W., Sciare, J., Lutz, M., Moukhtar, S., and Wagener, S.: New Directions: Time to

33   tackle urban wood burning?, Atmos. Environ., 68, 295-296, 2013.

Atmospheric
Chemistry
and Physics
Discussions

Open Access

EGU

1   Fuzzi, S., Baltensperger, U., Carslaw, K., Decesari, S., van der Gon, H. D., Facchini, M. C.,

2   Fowler, D., Koren, I., Langford, B., Lohmann, U., Nemitz, E., Pandis, S., Riipinen, I., Rudich,

3   Y., Schaap, M., Slowik, J. G., Spracklen, D. V., Vignati, E., Wild, M., Williams, M., and

4   Gilardoni, S.: Particulate matter, air quality and climate: lessons learned and future needs,

5   Atmos. Chem. Phys., 15, 8217-8299, 2015.

6   Gariazzo, C., Argentini, S., Balducci, C., Bogliolo, M. P., Cecinato, A., Cesaroni, G.,

7   Cristofari, A., D'Allura, A., Finardi, S., Forastiere, F., Gatto, M. P., Gherardi, M., Gordiani,

8   A., Hänninen, O., Lamberti, M., Pelliccioni, A., Perilli, M., Perrino, C., Porta, D., Radice, P.,

9   Romagnoli, P., Sacco, F., Silibello, C., Stafoggia, M., and Tofful, L.: Biomass burning

10   contribution to PAHs concentration in the urban area of Rome. Main findings from the LIFE+

11   EXPAH project and further observations., 10th International Conference on Air Quality -

12   Science and Application, Milan, Italy, 2016.

13   Gobbi, G. P., Angelini, F., Barnaba, F., Costabile, F., Baldasano, J. M., Basart, S., Sozzi, R.,

14   and Bolignano, A.: Changes in particulate matter physical properties during Saharan

15   advections over Rome (Italy): a four-year study, 2001-2004, Atmos. Chem. Phys., 13, 7395-

16   7404, 2013.

17   Gobbi, G. P., Barnaba, F., and Ammannato, L.: The vertical distribution of aerosols, Saharan

18   dust and cirrus clouds in Rome (Italy) in the year 2001, Atmos. Chem. Phys., 4, 351–359,

19   2004.

20   Harrison, R. M., Grenfell, J. L., Savage, N., Allen, A., Clemitshaw, K. C., Penkett, S., Hewitt,

21   C. N., and Davison, B.: Observations of new particle production in the atmosphere of a

22   moderately polluted site in eastern England, J. Geophys. Res.-Atmos., 105, 17819-17832,

23   2000.

24   Heal, M. R., Kumar, P., and Harrison, R. M.: Particles, air quality, policy and health,

25   Chemical Society Reviews, 41, 6606-6630, 2012.

26   Hildemann, L. M., Markowski, G. R., and Cass, G. R.: Chemical composition of emissions

27   from urban sources of fine organic aerosol, Environ. Sci. Technol., 25, 744-759, 1991.

28   Jacob III, P. and Byrd, G. D.: Chapter 6 - Use of gas chromatographic and mass spectrometric

29   techniques for the determination of nicotine and its metabolites. In: Analytical Determination

30   of Nicotine and Related Compounds and their Metabolites, Elsevier Science, Amsterdam,

31   1999.

32   Jayne, J. T., Leard, D. C., Zhang, X., Davidovits, P., Smith, K. A., Kolb, C. E., and

33   D.R.Worsnop: Development of an Aerosol Mass Spectrometer for Size and Composition

34   Analysis of Submicron Particles, Aerosol Science and Technology, 33, 49-70, 2000.

Atmospheric
Chemistry
and Physics
Discussions

Open Access

EGU

1 Jimenez, J. L., Canagaratna, M. R., Donahue, N. M., Prevot, A. S. H., Zhang, Q., Kroll, J. H.,

2 DeCarlo, P. F., Allan, J. D., Coe, H., Ng, N. L., Aiken, A. C., Docherty, K. S., Ulbrich, I. M.,

3 Grieshop, A. P., Robinson, A. L., Duplissy, J., Smith, J. D., Wilson, K. R., Lanz, V. A.,

4 Hueglin, C., Sun, Y. L., Tian, J., Laaksonen, A., Raatikainen, T., Rautiainen, J., Vaattovaara,

5 P., Ehn, M., Kulmala, M., Tomlinson, J. M., Collins, D. R., Cubison, M. J., Dunlea, E. J.,

6 Huffman, J. A., Onasch, T. B., Alfarra, M. R., Williams, P. I., Bower, K., Kondo, Y.,

7 Schneider, J., Drewnick, F., Borrmann, S., Weimer, S., Demerjian, K., Salcedo, D., Cottrell,

8 L., Griffin, R., Takami, A., Miyoshi, T., Hatakeyama, S., Shimono, A., Sun, J. Y., Zhang, Y.

9 M., Dzepina, K., Kimmel, J. R., Sueper, D., Jayne, J. T., Herndon, S. C., Trimborn, A. M.,

10 Williams, L. R., Wood, E. C., Middlebrook, A. M., Kolb, C. E., Baltensperger, U., and

11 Worsnop, D. R.: Evolution of Organic Aerosols in the Atmosphere, Science, 326, 1525-1529,

12 2009.

13 Kallos, G., Nickovic, S., Papadopoulos, A., Jovic, D., Kakaliagou, O., Misirlis, N., Boukas,

14 L., Mimikou, N., Sakellaridis, G., Papageorgiou, J., Anadranistakis, E., and Manousakis, M.:

15 The regional weather forecasting system SKIRON: An overview, paper presented at the

16 International Symposium on Regional Weather Prediction on Parallel Computer

17 Environments, University of Athens, Athens, Greece, 15-17 Oct. 1997.

18 Kulmala, M. and Kerminen, V.-M.: On the formation and growth of atmospheric

19 nanoparticles, Atmospheric Research, 90, 132-150, 2008.

20 Lanz, V. A., Alfarra, M. R., Baltensperger, U., Buchmann, B., Hueglin, C., and Prevot, A. S.

21 H.: Source apportionment of submicron organic aerosols at an urban site by factor analytical

22 modelling of aerosol mass spectra, Atmos. Chem. Phys., 7, 1503-1522, 2007.

23 Lanz, V. A., Prevot, A. S. H., Alfarra, M. R., Weimer, S., Mohr, C., DeCarlo, P. F., Gianini,

24 M. F. D., Hueglin, C., Schneider, J., Favez, O., D'Anna, B., George, C., and Baltensperger,

25 U.: Characterization of aerosol chemical composition with aerosol mass spectrometry in

26 Central Europe: an overview, Atmos. Chem. Phys., 10, 10453-10471, 2010.

27 Lucarelli, F., Calzolai, G., Chiari, M., Giannoni, M., Mochi, D., Nava, S., and Carraresi, L.:

28 The upgraded external-beam PIXE/PIGE set-up at LABEC for very fast measurements on

29 aerosol samples, Nuclear Instruments & Methods in Physics Research Section B-Beam

30 Interactions with Materials and Atoms, 318, 55-59, 2014.

31 Minguillon, M. C., Brines, M., Perez, N., Reche, C., Pandolfi, M., Fonseca, A. S., Amato, F.,

32 Alastuey, A., Lyasota, A., Codina, B., Lee, H. K., Eun, H. R., Ahn, K. H., and Querol, X.:

33 New particle formation at ground level and in the vertical column over the Barcelona area,

34 Atmospheric Research, 164, 118-130, 2015.

1   Mohr, C., DeCarlo, P. F., Heringa, M. F., Chirico, R., Slowik, J. G., Richter, R., Reche, C.,

2   Alastuey, A., Querol, X., Seco, R., Penuelas, J., Jimenez, J. L., Crippa, M., Zimmermann, R.,

3   Baltensperger, U., and Prevot, A. S. H.: Identification and quantification of organic aerosol

4   from cooking and other sources in Barcelona using aerosol mass spectrometer data, Atmos.

5   Chem. Phys., 12, 1649-1665, 2012.

6   Mohr, C., Huffman, J. A., Cubison, M. J., Aiken, A. C., Docherty, K. S., Kimmel, J. R.,

7   Ulbrich, I. M., Hannigan, M., and Jimenez, J. L.: Characterization of Primary Organic

8   Aerosol Emissions from Meat Cooking, Trash Burning, and Motor Vehicles with High-

9   Resolution Aerosol Mass Spectrometry and Comparison with Ambient and Chamber

10   Observations, Environ. Sci. Technol., 43, 2443-2449, 2009.

11   Ng, N. L., Canagaratna, M. R., Zhang, Q., Jimenez, J. L., Tian, J., Ulbrich, I. M., Kroll, J. H.,

12   Docherty, K. S., Chhabra, P. S., Bahreini, R., Murphy, S. M., Seinfeld, J. H., Hildebrandt, L.,

13   Donahue, N. M., DeCarlo, P. F., Lanz, V. A., Prevot, A. S. H., Dinar, E., Rudich, Y., and

14   Worsnop, D. R.: Organic aerosol components observed in Northern Hemispheric datasets

15   from Aerosol Mass Spectrometry, Atmos. Chem. Phys., 10, 4625-4641, 2010.

16   Paatero, P. and Tapper, U.: Positive matrix factorization: A non-negative factor model with

17   optimal utilization of error estimates of data values, Environmetrics, 5, 111-126, 1994.

18   Perez, C., Nickovic, S., Baldasano, J. M., Sicard, M., Rocadenbosch, F., and Cachorro, V. E.:

19   A long Saharan dust event over the western Mediterranean: Lidar, Sun photometer

20   observations, and regional dust modeling, J. Geophys. Res.-Atmos., 111, 2006a.

21   Perez, C., Nickovic, S., Pejanovic, G., Baldasano, J. M., and Oezsoy, E.: Interactive dust-

22   radiation modeling: A step to improve weather forecasts, J. Geophys. Res.-Atmos., 111,

23   2006b.

24   Pikridas, M., Sciare, J., Freutel, F., Crumeyrolle, S., von der Weiden-Reinmüller, S. L.,

25   Borbon, A., Schwarzenboeck, A., Merkel, M., Crippa, M., Kostenidou, E., Psichoudaki, M.,

26   Hildebrandt, L., Engelhart, G. J., Petäjä, T., Prévôt, A. S. H., Drewnick, F., Baltensperger, U.,

27   Wiedensohler, A., Kulmala, M., Beekmann, M., and Pandis, S. N.: In situ formation and

28   spatial variability of particle number concentration in a European megacity, Atmos. Chem.

29   Phys., 15, 10219-10237, 2015.

30   Reche, C., Querol, X., Alastuey, A., Viana, M., Pey, J., Moreno, T., Rodriguez, S., Gonzalez,

31   Y., Fernandez-Camacho, R., Sanchez de la Campa, A. M., de la Rosa, J., Dall'Osto, M.,

32   Prevot, A. S. H., Hueglin, C., Harrison, R. M., and Quincey, P.: New considerations for PM,

33   Black Carbon and particle number concentration for air quality monitoring across different

34   European cities, Atmos. Chem. Phys., 11, 6207-6227, 2011.

Atmospheric
Chemistry
and Physics
Discussions

1 Reche, C., Viana, M., Amato, F., Alastuey, A., Moreno, T., Hillamo, R., Teinila, K., Saarnio,

2 K., Seco, R., Penuelas, J., Mohr, C., Prevot, A. S. H., and Querol, X.: Biomass burning

3 contributions to urban aerosols in a coastal Mediterranean City, Sci. Total Environ., 427, 175-

4 190, 2012.

5 Rogge, W. F., Hildemann, L. M., Mazurek, M. A., and Cass, G. R.: Sources of Fine Organic

6 Aerosol. 6. Cigarette Smoke in the Urban Atmosphere, Environ. Sci. Technol., 28, 1375-

7 1388, 1994.

8 Schneider, J., Weimer, S., Drewnick, F., Borrmann, S., Helas, G., Gwaze, P., Schmid, O.,

9 Andreae, M. O., and Kirchner, U.: Mass spectrometric analysis and aerodynamic properties of

10 various types of combustion-related aerosol particles, International Journal of Mass

11 Spectrometry, 258, 37-49, 2006.

12 Shi, J. P., Evans, D. E., Khan, A. A., and Harrison, R. M.: Sources and concentration of

13 nanoparticles (< 10 nm diameter) in the urban atmosphere, Atmos. Environ., 35, 1193-1202,

14 2001.

15 Sibson, R.: A brief description of natural neighbour interpolation. In: Interpreting Multivariate

16 Data, Barnett, I. V. (Ed.), Wiley, New York, USA, 1981.

17 Srivastava, M. K. and Sarthi, P. P.: Turbulent kinetic energy in the atmospheric surface layer

18 during the summer monsoon, Meteorological Applications, 9, 239-246, 2002.

19 Stafoggia, M., Zauli-Sajani, S., Pey, J., Samoli, E., Alessandrini, E., Basagana, X.,

20 Cernigliaro, A., Chiusolo, M., Demaria, M., Diaz, J., Faustini, A., Katsouyanni, K., Kelessis,

21 A. G., Linares, C., Marchesi, S., Medina, S., Pandolfi, P., Perez, N., Querol, X., Randi, G.,

22 Ranzi, A., Tobias, A., Forastiere, F., and Grp, M.-P. S.: Desert Dust Outbreaks in Southern

23 Europe: Contribution to Daily PM10 Concentrations and Short-Term Associations with

24 Mortality and Hospital Admissions, Environmental Health Perspectives, 124, 413-419, 2016.

25 Stein, A. F., Draxler, R. R., Rolph, G. D., Stunder, B. J. B., Cohen, M. D., and Ngan, F.:

26 NOAA's HYSPLIT Atmospheric Transport and Dispersion Modeling System, Bulletin of the

27 American Meteorological Society, 96, 2059-2077, 2015.

28 Stohl, A., Forster, C., Frank, A., Seibert, P., and Wotawa, G.: Technical note: The Lagrangian

29 particle dispersion model FLEXPART version 6.2, Atmos. Chem. Phys., 5, 2461-2474, 2005.

30 Ulbrich, I. M., Canagaratna, M. R., Zhang, Q., Worsnop, D. R., and Jimenez, J. L.:

31 Interpretation of organic components from Positive Matrix Factorization of aerosol mass

32 spectrometric data, Atmos. Chem. Phys., 9, 2891-2918, 2009.

Atmospheric
Chemistry
and Physics
Discussions

Open Access

EGU

1   Weimer, S., Alfarra, M. R., Schreiber, D., Mohr, M., Prevot, A. S. H., and Baltensperger, U.:

2   Organic aerosol mass spectral signatures from wood-burning emissions: Influence of burning

3   conditions and wood type, J. Geophys. Res.-Atmos., 113, 2008.

4   Yu, K. N., Cheung, Y. P., Cheung, T., and Henry, R. C.: Identifying the impact of large urban

5   airports on local air quality by nonparametric regression, Atmos. Environ., 38, 4501-4507,

6   2004.

7   Zhang, Q., Jimenez, J. L., Canagaratna, M. R., Ulbrich, I. M., Ng, N. L., Worsnop, D. R., and

8   Sun, Y.: Understanding atmospheric organic aerosols via factor analysis of aerosol mass

9   spectrometry: a review, Anal. Bioanal. Chem., 401, 3045-3067, 2011.

10 Zhang, Q., Stanier, C. O., Canagaratna, M. R., Jayne, J. T., Worsnop, D. R., Pandis, S. N., and

11 Jimenez, J. L.: Insights into the chemistry of new particle formation and growth events in

12 Pittsburgh based on aerosol mass spectrometry, Environ. Sci. Technol., 38, 4797-4809, 2004.

13 Zheng, M., Salmon, L. G., Schauer, J. J., Zeng, L. M., Kiang, C. S., Zhang, Y. H., and Cass,

14 G. R.: Seasonal trends in PM2.5 source contributions in Beijing, China, Atmos. Environ., 39,

15 3967-3976, 2005.

16

Atmospheric
Chemistry
and Physics
Discussions

1   Table 1. Summary of measurement campaigns and measurement periods.

Campaign name	Measurement location	Classification	Measurement period
DIAPASON2013	Tor Vergata	Urban background	23.10. – 07.11.2013
POPE2013	Central Rome	Urban	07.11. – 14.11.2013
DIAPASON2014	Tor Vergata	Urban background	20.05. – 04.06.2014
POPE2014	Central Rome	Urban	04.06. – 17.06.2014

2

Atmospheric
Chemistry
and Physics
Discussions

1   Table 2. Summary of the instruments deployed in MoLa during all measurement periods,

2   together with measured variables. D_p: particle diameter (defined according to individual

3   instrumental measurement method: optical, aerodynamic, or mobility diameter).

Instrument	Measured variable
Chemical composition of PM$_1$	
Aerosol mass spectrometer (HR-ToF-AMS)	Organics, sulphate, nitrate, ammonium, chloride (non-refractory) mass concentrations (D_p = ~ 70 – 800 nm)
Multi Angle Absorption Photometer (MAAP)	Black carbon (BC) mass concentration
PAS2000	Particulate PAH[a] mass concentration
Physical aerosol properties	
Condensation particle counter (CPC)	Total number concentration (D_p > 2.5 nm)
Fast mobility particle sizer (FMPS)	Size distribution (D_p = 5.6 – 560 nm)
Optical particle counter (OPC)[b]	Size distribution (D_p = 0.25 – 32 µm)
Aerodynamic particle sizer (APS)	Size distribution (D_p = 0.5 – 20 µm)
Environmental Dust Monitor (EDM)	Mass concentration of PM$_1$, PM$_{2.5}$, PM$_{10}$
Trace gas mixing ratios	
Airpointer	NO$_2$, NO$_x$, NO, SO$_2$, CO, O$_3$
LI-840	H$_2$O, CO$_2$
Meteorology	
Meteorological station[c]	Wind direction, wind speed, temperature, pressure, solar radiation, precipitation, relative humidity

4   [a] Polycyclic Aromatic Hydrocarbons

5   [b] No data collected during DIAPASON2014.

6   [c] Wind direction, wind speed and solar radiation data not useable during POPE measurements.

Atmospheric
Chemistry
and Physics
Discussions

Open Access

EGU

1   Table 3. Summary of selected variables measured during DIAPASON (Tor Vergata) and

2   POPE (central Rome) in 2013 and 2014. Values represent total campaign averages, calculated

3   from 5 min averages, and their standard deviations. N/A: not available.

	DIAPASON2013 (Oct/Nov 2013)	POPE2013 (Nov 2013)	DIAPASON2014 (May/June 2014)	POPE2014 (June 2014)
Temperature / $^\circ$ C	17.6 ± 2.9	16.1 ± 2.8	19.0 ± 3.5	24.9 ± 4.5
Rain [a] / mm	46.3 (5)	25.9 (6)	6.3 (5)	69.9 (4)
Pressure / hPa	1004 ± 7	1009 ± 6	1002 ± 2	1012 ± 4
Solar radiation [b] / W m^{-2}	103 ± 26	N/A	282 ± 55	N/A
Rel. humidity / %	78 ± 11	73 ± 6	61 ± 15	52 ± 16
Wind speed / m s^{-1}	1.9 ± 1.3	N/A	2.5 ± 1.6	N/A
Daily BLH [c] max. / m	850 ± 220	900 ± 150	1500 ± 450	1560 ± 250
TKE [d] / J kg^{-1}	0.48 ± 0.45	1.8 ± 2.3	0.84 ± 0.79	0.68 ± 0.52
PM_{10} / µg m^{-3}	22 ± 12	13 ± 7	15 ± 8	17 ± 8
$PM_{10-2.5}$ [e] / µg m^{-3}	4.5 ± 3.1	4.7 ± 3.2	9.3 ± 6.5	7.1 ± 5.7
PM_1 / µg m^{-3}	15 ± 10	6.0 ± 3.6	5.8 ± 3.5	7.5 ± 3.8
PNC / 10^3 cm^{-3}	23 ± 15	27 ± 11	18 ± 10	13 ± 5
NO_x / ppb	29 ± 27	36 ± 27	9 ± 9	13 ± 8
CO_2 / ppm	410 ± 20	420 ± 20	410 ± 20	420 ± 20
O_3 / ppb	14 ± 14	8.9 ± 10	34 ± 19	35 ± 22
PAH / ng m^{-3}	45 ± 54	45 ± 39	10 ± 14	12 ± 11
Org [f] / µg m^{-3}	5.3 ± 4.5	2.5 ± 1.8	4.5 ± 3.2	6.6 ± 3.3
SO_4 / µg m^{-3}	2.0 ± 1.1	0.48 ± 0.44	1.6 ± 0.44	2.6 ± 1.3

NO_3 / $\mu g\ m^{-3}$	0.86 ± 0.80	0.23 ± 0.17	0.61 ± 0.72	0.49 ± 0.40
NH_4 / $\mu g\ m^{-3}$	0.88 ± 0.48	0.20 ± 0.18	0.66 ± 0.27	0.97 ± 0.46
Chl / $\mu g\ m^{-3}$	0.09 ± 0.16	0.04 ± 0.06	0.06 ± 0.13	0.03 ± 0.08
BC / $\mu g\ m^{-3}$	2.9 ± 2.5	2.2 ± 1.7	1.3 ± 1.0	1.8 ± 1.0

1   [a] Total accumulated amount of rain during measurements. Numbers of days with rain are given in parentheses.

2   [b] Average and standard deviation of daily means. Only days with 24 h measurements were used (includes 85 % of data).

3   [c] Average and standard deviation of daily boundary layer height (BLH) maxima from polarization LIDAR-ceilometer.

4   measurements at the Tor Vergata site provided by the DIAPASON project (DIAPASON, 2016).

5   [d] Turbulent kinetic energy (TKE) calculated from 2-hour averages provided by Arpa Lazio Environmental Agency from

6   measurements at 3 sites around Rome (Tor Vergata, Castel di Guido, Boncompagni).

7   [e] Difference between PM_{10} and $PM_{2.5}$ (coarse particles).

8   [f] For POPE2013 and POPE2014 corrected for contribution from local cigarette smoke emissions, compare Sect. 4.2.5.

Atmospheric
Chemistry
and Physics
Discussions

Open Access
EGU

1   Table 4: Estimated contribution of "home-made" and "advected" species to total PM_1 for all

2   measurement periods. Dust advection periods and emissions from cigarettes are excluded.

	Home-made PM_1 / $\mu g\ m^{-3}$ (contribution to PM_1 / %)	Advected PM_1 / $\mu g\ m^{-3}$ (contribution to PM_1 / %)
DIAPASON2013	6.5 (47)	7.3 (53)
POPE2013	3.9 (70)	1.7 (30)
DIAPASON2014	4.7 (59)	3.3 (41)
POPE2014	5.2 (42)	7.3 (58)

3

Atmospheric
Chemistry
and Physics

Discussions

1   Table 5. Summary of "dust" and "no dust" periods identified during DIAPASON2013 and

2   DIAPASON2014, including mean values and standard deviation of $PM_{10\text{-}2.5}$ and PM_{10}.

	DIAPASON2013		DIAPASON2014	
	Dust	No dust	Dust	No dust
Period	29.10.-01.11.13	23.10.-28.10.13; 02.11.-07.11.13	20.05.-26.05.14	27.05.-04.06.14
Mean $PM_{10\text{-}2.5}$ / $\mu g\ m^{-3}$	7.1 ± 3.5	4.0 ± 2.7	15.4 ± 5.9	5.5 ± 2.8
Mean PM_{10} / $\mu g\ m^{-3}$	32 ± 7	19 ± 12	22 ± 7	11 ± 5
Fraction of PM_{10} in PM_1	70 %	68 %	31 %	48 %

3

41

Atmospheric
Chemistry
and Physics
Discussions

1 Table 6. Variables measured during DIAPASON2014 indicating different ambient conditions

2 on days classified as "nucleation", "non-defined" and "non-nucleation" days. Total particle

3 number concentrations (PNC) and the classification criteria and number of respectively

4 classified days are also listed. For each measurement day and presented variable daily

5 averages for the period 10 am – 4 pm were calculated. Here, mean and standard deviation of

6 these averages are shown with maximum values coloured in red, minimum values coloured in

7 green.

	Nucleation days	Non-defined days	Non-nucleation days
Classification	$PNC_{nuc}/PNC_{bg} \geq 1.5$	$1 < PNC_{nuc}/PNC_{bg} < 1.5$	$PNC_{nuc}/PNC_{bg} \leq 1$
Number of days	6	6	2
Rain [a] / mm	0 (0)	0.7 (1)	2.3 (1)
Total PNC / 10^3 cm^{-3}	25 ± 9	13 ± 3	12 ± 1
Temperature / ° C	23 ± 2	22 ± 2	20 ± 0
Rel. humidity / %	43 ± 6	46 ± 9	56 ± 4
Solar radiation / W m^{-2}	780 ± 80	700 ± 190	670 ± 200
O_3 / ppb	54 ± 4	47 ± 6	48 ± 1
Total PM$_1$ organics / µg m^{-3}	3.9 ± 2.4	3.6 ± 1.0	2.9 ± 2.3

8 [a] Total accumulated amount of rain (10 am – 4 pm). Numbers of days with rain are given in parentheses.
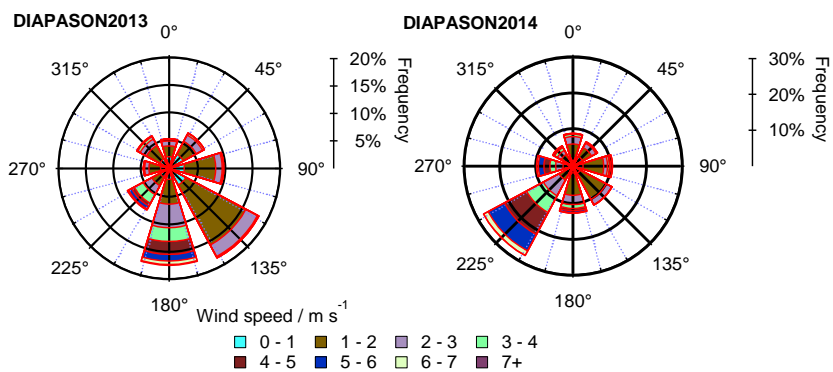
1

2   Figure 1. Relative frequency of local wind directions (in °) colour coded with wind speed

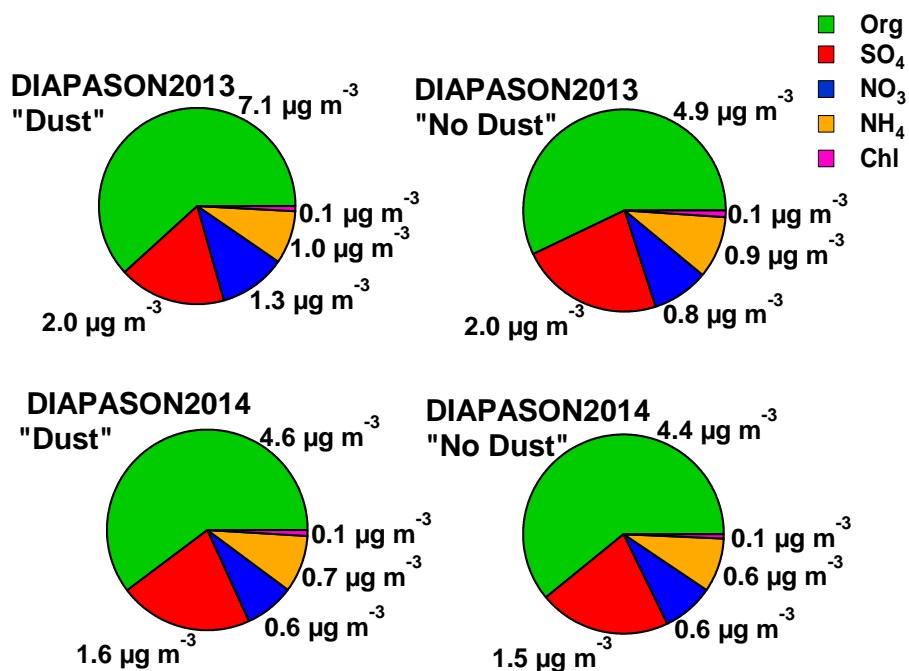3   measured during DIAPASON2013 (left) and DIAPASON2014 (right).

Atmospheric
Chemistry
and Physics
Discussions

EGU
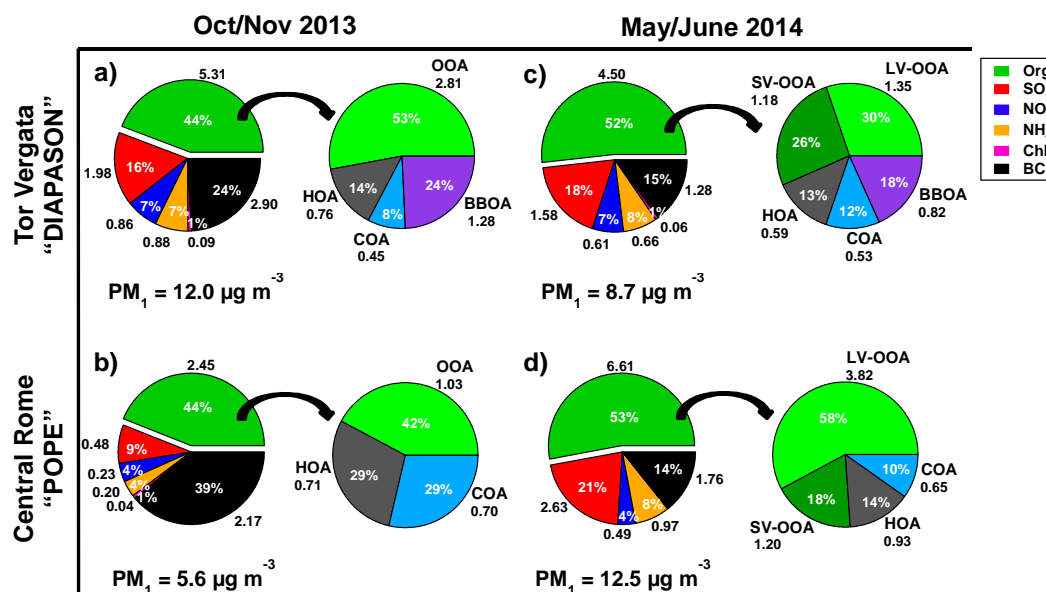
Figure 2. Mean chemical composition ($\mu g\ m^{-3}$) of non-refractory PM_1 together with BC (left chart in panels a-d) and PMF-separated organic fraction (right chart in panels a-d) for each measurement period. PM_1 values below the pie charts represent total mass concentration of AMS-measured species plus BC. The organic fraction measured at central Rome was corrected for contributions from cigarette smoke in the local environment (Sect. 4.2.5, also omitted from the pie charts depicting the PMF-separated organic fraction).

Atmospheric
Chemistry
and Physics
Discussions

Open Access

1
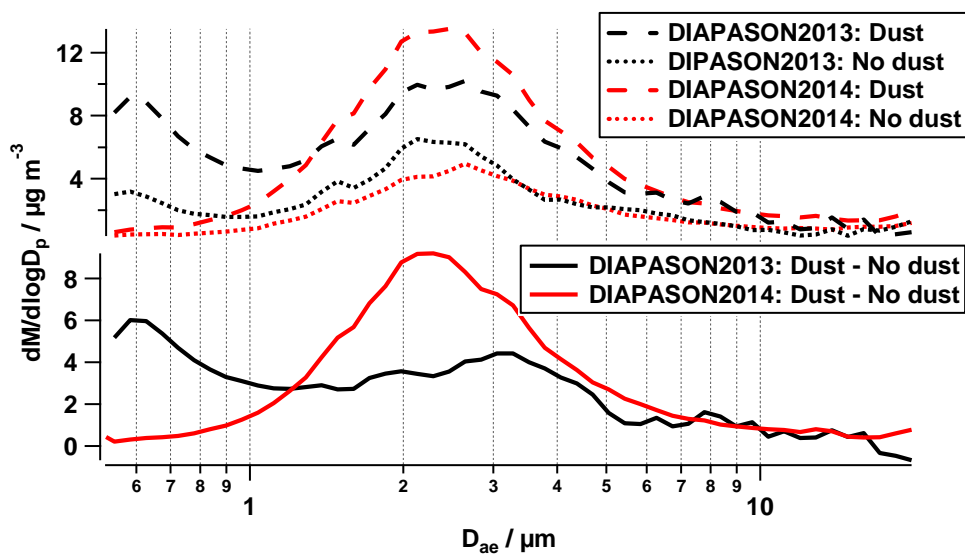
Figure 3. Size-resolved mass distribution (dM/dlogD$_p$) during "dust" (dashed traces) and "no dust" (dotted traces) periods (top panel) measured with the APS during DIAPASON2013 (black traces) and DIAPASON2014 (red traces). The difference of the size-resolved mass distributions measured during "dust" and "no dust" periods indicate the size distributions of the dust particles measured during both years (bottom panel). D$_{ae}$ is the aerodynamic particle diameter.

1

2 Figure 4. Comparison of mean chemical composition of non-refractory PM_1 obtained from

3 AMS measurements during "dust" (left) and "no dust" (right) periods during

4 DIAPASON2013 (top) and DIAPASON2014 (bottom).

Atmospheric
Chemistry
and Physics
Discussions
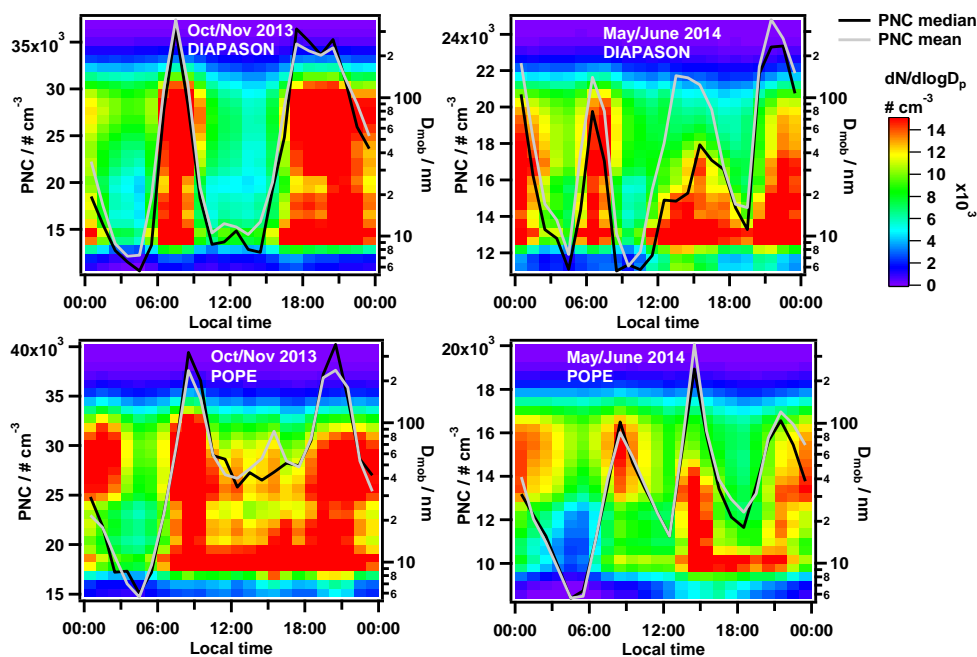
1

2   Figure 5. Average diurnal cycles of particle number concentrations and size distributions for

3   DIAPASON (top) and POPE (bottom) for each year (left: 2013, right: 2014). Image plots of

4   diurnal cycles of the particle number size distributions (colour coded for dN/dlogD$_p$) are

5   shown with the particle diameters on the right axes (mobility particle diameter D$_{mob}$). Mean

6   (grey) and median (black) diurnal cycles of the total particle number concentrations are shown

7   on the left axes. New particle formation at midday was only observed in the May/June 2014

8   campaigns.

Atmospheric
Chemistry
and Physics
Discussions

Open Access

1
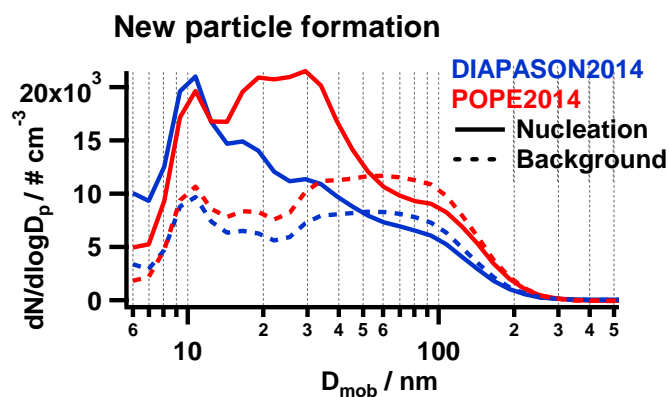
Figure 6. Average size distributions of particle number concentrations (dN/dlogD$_p$) for maximum PNC at midday (DIAPASON2014: 1-3 pm; POPE2014: 2-3 pm; solid traces) and during background conditions (10-11 am; dashed traces) from FMPS measurements for DIAPASON2014 (blue) and POPE2014 (red). D$_{mob}$ is the mobility diameter.

Atmospheric
Chemistry
and Physics
Discussions
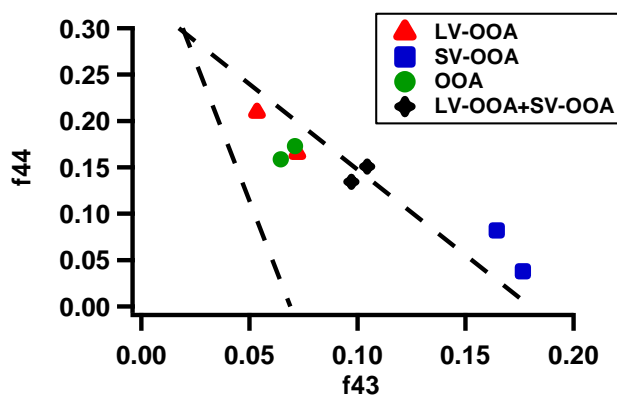
1

2 Figure 7. f44 vs. f43 plotted for each OOA factor obtained from PMF analysis of the organic

3 fraction of HR-AMS data. OOA factors (green markers) resulted from DIAPASON2013 and

4 POPE2013 measurements; SV-OOA (blue markers) and LV-OOA factors (red markers) were

5 found during DIAPASON2014 and POPE2014 measurements. The recombination of the

6 factors LV-OOA and SV-OOA for both DIAPASON2014 and POPE2014 is also shown

7 (black markers). The dashed lines represent the triangular space in which measured ambient

8 OOA components typically cluster according to Ng et al. (2010).
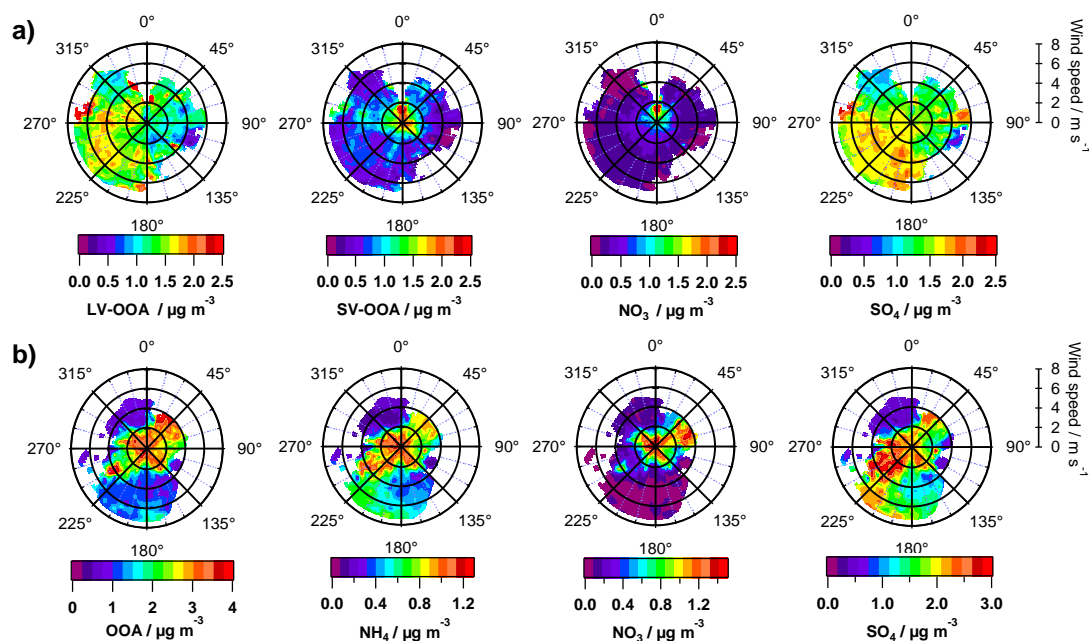
Figure 8. Polar plots of (a) submicron LV-OOA, SV-OOA, NO$_3$ and SO$_4$ concentration (colour coded) obtained from DIAPASON2014 measurements and (b) submicron OOA, NH$_4$, NO$_3$ and SO$_4$ concentration obtained from DIAPASON2013 measurements as a function of local wind direction (°) and speed (m s^{-1}).
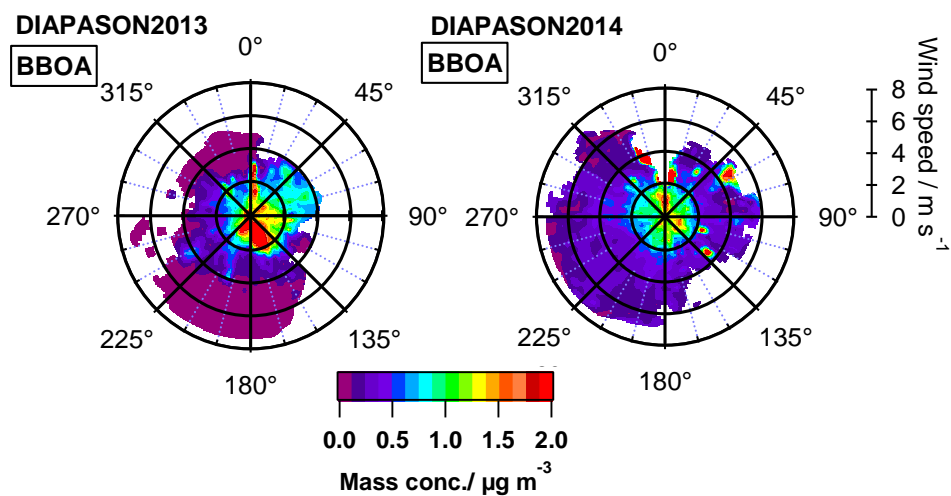
1

2   Figure 9. Submicron BBOA mass concentrations (colour coded) as a function of local wind

3   direction (°) and speed (m s^{-1}) for DIAPASON2013 (left) and DIAPASON2014 (right).
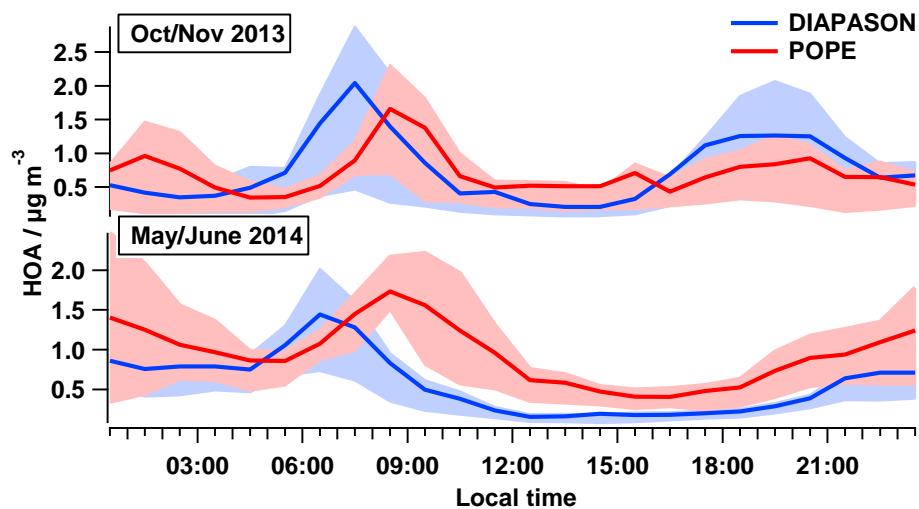
1

2   Figure 10. Diurnal cycles of HOA mass concentrations obtained from measurements at Tor

3   Vergata (blue; DIAPASON) and central Rome (red; POPE) during both seasons. Shown are

4   mean concentrations (traces) and the corresponding 25th and 75th percentiles (shaded areas).

Atmospheric
Chemistry
and Physics
Discussions

Open Access
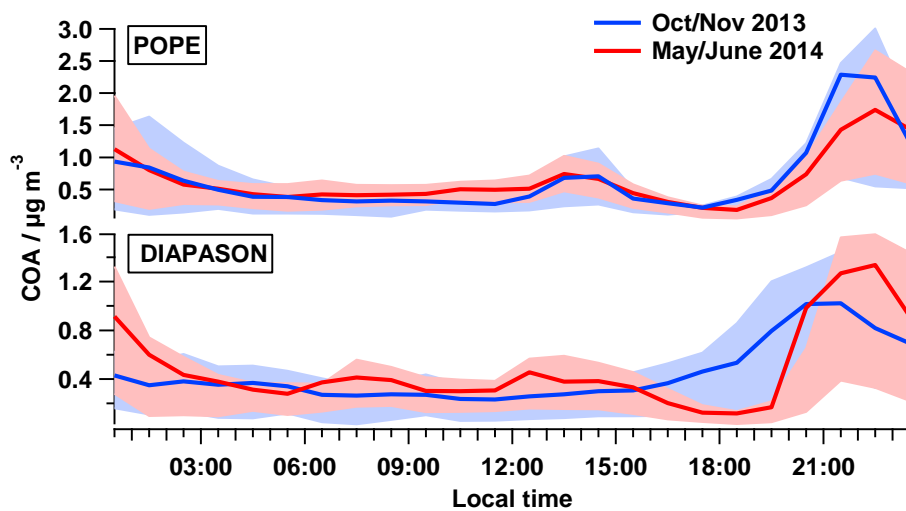
1

2 Figure 11. Diurnal cycles of COA mass concentrations observed at central Rome (top; POPE)

3 and the suburban site (bottom; DIAPASON) during both seasons. Shown are mean

4 concentrations (traces) and the corresponding 25th and 75th percentiles (shaded areas).
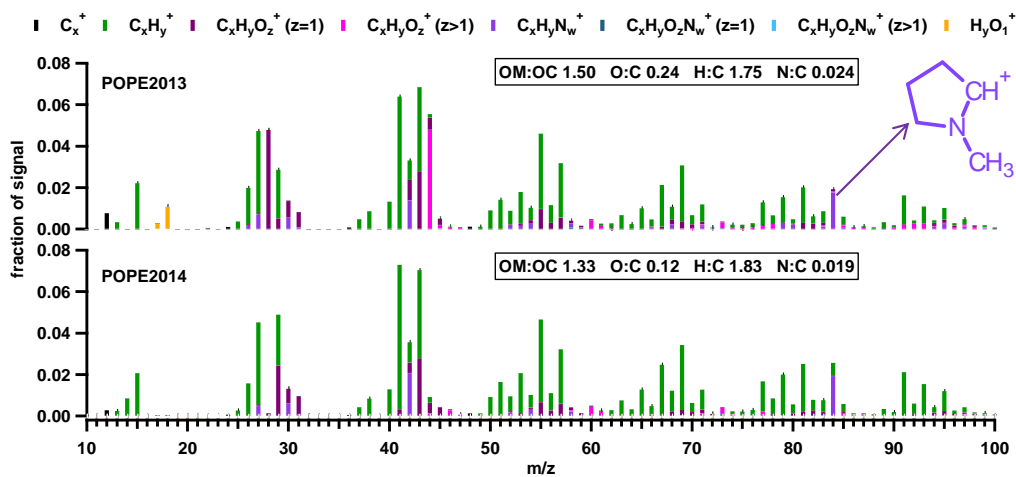
1

2 Figure 12. Unit mass resolution spectra of CSOA obtained for the two POPE campaigns,

3 calculated from organic high resolution mass spectra and colour coded for the different groups

4 of ion fragments. The elemental ratios are shown in boxes. The chemical structure of the

5 suggested ion fragment at m/z 84 ($C_5H_{10}N^+$) is also illustrated.
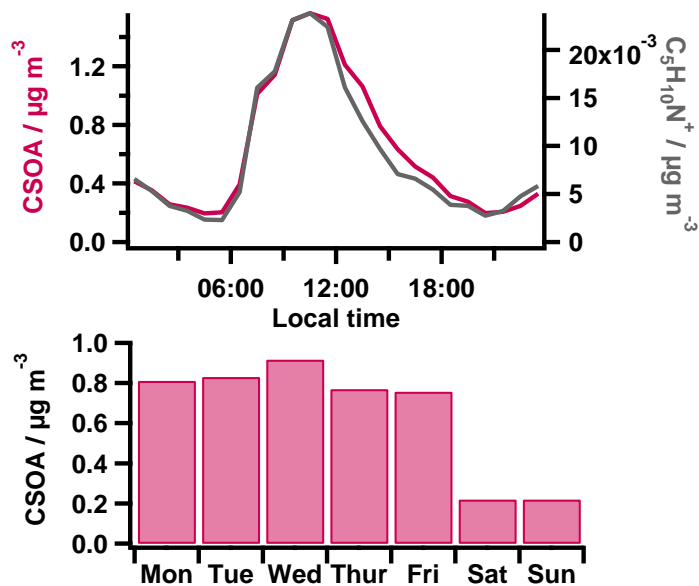
1

2   Figure 13. Diurnal cycle of CSOA and the marker fragment $C_5H_{10}N^+$ (top) and the weekly

3   cycle (bottom) of CSOA mass concentrations obtained from HR-AMS data of POPE2014.